AFRL-SN-HS-TR-2004-044

TRAVELING ELECTROMAGNETIC WAVES ON LINEAR PERIODIC ARRAYS OF SMALL LOSSLESS PENETRABLE SPHERES

Dr. Robert A. Shore
Dr. Arthur Yaghjian (Visiting Scientist)
Antenna Technology Branch
Electromagnetics Technology Division
AFRL/SNHA

IN-HOUSE REPORT January 2003 – June 2004

AIR FORCE RESEARCH LABORATORY
Sensors Directorate
Electromagnetics Technology Division
80 Scott Drive
Hanscom AFB MA 01731-2909

TECHNICAL REPORT

Title: Traveling Electromagnetic Waves on Linear Periodic Arrays of Small Lossless Penetrable Spheres

Unlimited, Statement A

NOTICE

USING GOVERNMENT DRAWINGS, SPECIFICATIONS, OR OTHER DATA INCLUDED IN THIS DOCUMENT FOR ANY PURPOSE OTHER THAN GOVERNMENT PROCUREMENT DOES NOT IN ANY WAY OBLIGATE THE US GOVERNMENT. THE FACT THAT THE GOVERNMENT FORMULATED OR SUPPLIED THE DRAWINGS, SPECIFICATIONS, OR OTHER DATA DOES NOT LICENSE THE HOLDER OR ANY OTHER PERSON OR CORPORATION; OR CONVEY ANY RIGHTS OR PERMISSION TO MANUFACTURE, USE, OR SELL ANY PATENTED INVENTION THAT MAY RELATE TO THEM.

THIS TECHNICAL REPORT HAS BEEN REVIEWED AND IS APPROVED FOR PUBLICATION.

//signature//

Robert Shore/SNHA/2058
Project Manager

//signature//

Livio Poles/SNHA/4087
Branch Chief

//signature//

Michael Alexander/SNH/4034
Technical Advisor

REPORT DOCUMENTATION PAGE

Form Approved OMB No. 0704-0188

1. REPORT DATE *(DD-MM-YYYY)*		3. DATES COVERED *(From - To)*
20-06-2004	IN-HOUSE	1 January 2003 – 1 June 2004

4. TITLE AND SUBTITLE
Traveling Electromagnetic Waves on Linear Periodic Arrays of Lossless Penetrable Spheres

5a. CONTRACT NUMBER

5b. GRANT NUMBER

5c. PROGRAM ELEMENT NUMBER
61102F

6. AUTHOR(S)
Robert A. Shore and Arthur D. Yaghjian

5d. PROJECT NUMBER
2304

5e. TASK NUMBER
HE

5f. WORK UNIT NUMBER
01

7. PERFORMING ORGANIZATION NAME(S) AND ADDRESS(ES)
AFRL/SNHA
80 Scott Drive
Hanscom AFB, MA 01731-2909

8. PERFORMING ORGANIZATION REPORT

9. SPONSORING / MONITORING AGENCY NAME(S) AND ADDRESS(ES)
Electromagnetics Technology Division
Sensors Directorate
Air Force Research Laboratory
80 Scott Drive
Hanscom AFB MA 01731-2909

10. SPONSOR/MONITOR'S ACRONYM(S)
AFRL/SNHA

11. SPONSOR/MONITOR'S REPORT NUMBER(S)

12. DISTRIBUTION / AVAILABILITY STATEMENT
Approved for public release; distribution unlimited.

13. SUPPLEMENTARY NOTES

14. ABSTRACT
Electromagnetic waves on infinite linear periodic arrays of lossless penetrable spheres can be conveniently analyzed using the source scattering-matrix framework and vector spherical wave functions. Our investigation of these arrays is motivated by the theoretical demonstration that a double negative (DNG) material can be formed by embedding an array of spherical particles in a background matrix. In this report we apply the spherical-wave source scattering-matrix approach to obtain an implicit transcendental equation for the propagation constants of the traveling waves that can be supported on infinite linear periodic arrays of lossless penetrable (magnetodielectric) spheres. Although a framework is presented for all orders of vector spherical waves, only the electric and magnetic dipole waves are included in the detailed analysis. The report focuses on determining the kd – βd diagrams for the traveling waves that can be supported. Backward waves and waves with low group velocity are shown to be supportable in narrow wavebands by arrays composed of spheres with appropriately chosen permittivity and permeability. Interestingly, for certain spheres and separations it is possible to have two or even three different dipolar traveling waves supported by the array.

15. SUBJECT TERMS
Linear arrays, scattering matrices, traveling waves, magnetodielectric spheres

16. SECURITY CLASSIFICATION OF:			17.LIMITATION OF ABSTRACT	18.NUMBER OF PAGES	19a. NAME OF RESPONSIBLE PERSON Dr. Robert A. Shore
a. REPORT Unclassified	b. ABSTRACT Unclassified	c.THIS PAGE Unclassified	SAR	41	19b. TELEPHONE NUMBER *(include area code)* *781-377-2058*

Standard Form 298 (Rev. 8-98)
Prescribed by ANSI Std. Z39.18

Contents

List of Figures

ACKNOWLEDGEMENT

This work was supported by the U.S. Air Force Office of Scientific Research (AFOSR).

1 INTRODUCTION

The spherical-wave source scattering-matrix description of electroacoustic transducers [1] and antennas [2] is ideally suited for the analysis of arrays of small radiators and scatterers. In [1], it formed the basis of the analysis that determined a simple, explicit, closed-form expression for the propagation constants ($kd - \beta d$ diagram) of the traveling waves on an infinite linear periodic array of isotropic acoustic scatterers. And in [2], it was applied to obtain implicit transcendental expressions for the $kd - \beta d$ diagrams of the traveling waves on infinite linear periodic arrays of electric (or magnetic) dipole scatterers oriented perpendicular, parallel, and skew to the direction of propagation of the traveling waves. The analyses in these two previous applications of the spherical-wave source scattering-matrix description simplified greatly by assuming the scatterers were small enough that only the fields with the lowest order radial dependence were significant.

In the present report, we apply the spherical-wave source scattering-matrix description to obtain an implicit transcendental equation for the propagation constants of the traveling waves that can exist on an infinite linear periodic array of lossless penetrable (magnetodielectric) spheres. Although a framework is presented for all orders of vector spherical waves, only the electric and magnetic dipole waves are included in the detailed analysis. The exclusion of higher-order vector spherical waves restricts the scope of this paper either to spheres sufficiently small that only the dipole scattered fields can be excited, or to frequencies for which all the scattered multipole fields are negligible except the dipole fields. In all the particular numerical examples we shall consider, the magnitudes of the dipole wave scattering coefficients are much larger than those of the higher-order multipole wave coefficients, and consequently the dipole vector spherical waves give an accurate description of the traveling waves that can exist on the array. It should be kept in mind, however, that there may well be traveling waves associated with the higher-order vector spherical waves for arrays of penetrable spheres in the general range of sizes we consider in some of our numerical examples. Although three-dimensional arrays of periodic penetrable spheres have been analyzed in the past [3], [4], [5], the present analysis concentrates on determining $kd - \beta d$ diagrams for the traveling waves on a single linear periodic array of penetrable spheres with arbitrary separation and arbitrary values of real permeability and permittivity.

The report begins with a brief review of the spherical-wave source scattering-matrix description of electromagnetic scatterers and then goes on to simplify the equations for spheres that involve only electric and magnetic dipole vector spherical waves. Next these simplified equations are applied to an infinite linear periodic array of these spheres. The resulting equations are combined, rearranged, and reduced to a single transcendental equation, which is solved numerically, to obtain $kd - \beta d$ diagrams for a number of different values of the relative permeability and permittivity of the spheres in the infinite linear array. Two-layered (coated) spheres are considered as well as homogeneous spheres. Notably, the $kd - \beta d$ diagrams predict that both forward and backward dipolar traveling waves can be excited on linear periodic arrays of penetrable spheres, depending on the frequency and the values of the permeability and permittivity of the spheres. In contrast, we showed in [2] that only forward traveling waves are possible on linear periodic arrays of unloaded short-wire dipoles.

2 SOURCE SCATTERING-MATRIX DESCRIPTION OF A GENERAL SCATTERER

Consider a general scatterer bounded by the surface S as pictured in Figure 1. The Maxwell equations that govern the time-harmonic electromagnetic fields ($e^{-i\omega t}, \omega > 0$) in the source-free free space between the surface S and a spherical surface S_r of radius r enclosing the scatterer and extending to the nearest external source are [6, sec. 7.1]

$$\nabla \times \mathbf{E}(\mathbf{r}) = ikZ_0\mathbf{H} \tag{1a}$$

$$\nabla \times \mathbf{H}(\mathbf{r}) = -ik\mathbf{E}(\mathbf{r})/Z_0 \tag{1b}$$

which imply that

$$\nabla \cdot \mathbf{E}(\mathbf{r}) = 0 \tag{2a}$$

$$\nabla \cdot \mathbf{H}(\mathbf{r}) = 0 \tag{2b}$$

where $\mathbf{E}(\mathbf{r})$ and $\mathbf{H}(\mathbf{r})$ are the electric and magnetic fields, Z_0 is the free space impedance, $k = \omega/c = 2\pi/\lambda$ is the free space propagation constant, λ is the free-space wavelength, and c is the speed of light. Eliminating either $\mathbf{H}(\mathbf{r})$ or $\mathbf{E}(\mathbf{r})$ from these equations yields the vector wave equations

$$-\nabla \times \nabla \times \mathbf{E}(\mathbf{r}) + k^2\mathbf{E}(\mathbf{r}) = 0 \tag{3a}$$

$$-\nabla \times \nabla \times \mathbf{H}(\mathbf{r}) + k^2\mathbf{H}(\mathbf{r}) = 0 \tag{3b}$$

which imply

$$\nabla^2\mathbf{E}(\mathbf{r}) + k^2\mathbf{E}(\mathbf{r}) = 0, \quad \nabla \cdot \mathbf{E}(\mathbf{r}) = 0 \tag{4a}$$

$$\nabla^2\mathbf{H}(\mathbf{r}) + k^2\mathbf{H}(\mathbf{r}) = 0, \quad \nabla \cdot \mathbf{H}(\mathbf{r}) = 0. \tag{4b}$$

Since the electric field satisfies (4a) in the source-free free space region between the surface S and the spherical surface S_r, the electric field in this region can be expanded in a complete set of divergenceless vector spherical wave functions [6],[7]

$$\mathbf{E}(\mathbf{r}) = \sum_{l=1}^{\infty}\sum_{m=-l}^{l}\left[a_{lm}^{(1)}\mathbf{M}_{lm}^{(1)}(\mathbf{r}) + b_{lm}^{(1)}\mathbf{M}_{lm}^{(2)}(\mathbf{r}) + a_{lm}^{(2)}\mathbf{N}_{lm}^{(1)}(\mathbf{r}) + b_{lm}^{(2)}\mathbf{N}_{lm}^{(2)}(\mathbf{r})\right]. \tag{5}$$

The spherical-wave expansion of the magnetic field then follows from (1a)

$$\mathbf{H}(\mathbf{r}) = -iY_0\sum_{l=1}^{\infty}\sum_{m=-l}^{l}\left[a_{lm}^{(1)}\mathbf{N}_{lm}^{(1)}(\mathbf{r}) + b_{lm}^{(1)}\mathbf{N}_{lm}^{(2)}(\mathbf{r}) + a_{lm}^{(2)}\mathbf{M}_{lm}^{(1)}(\mathbf{r}) + b_{lm}^{(2)}\mathbf{M}_{lm}^{(2)}(\mathbf{r})\right] \tag{6}$$

where $Y_0 = 1/Z_0$ is the free-space admittance. The vector spherical harmonics $\mathbf{M}_{lm}^{(i)}(\mathbf{r})$ and $\mathbf{N}_{lm}^{(i)}(\mathbf{r})$ are defined in Appendix A. They satisfy the equations

$$\mathbf{N}_{lm}^{(i)}(\mathbf{r}) = \frac{1}{k}\nabla \times \mathbf{M}_{lm}^{(i)}(\mathbf{r}) \tag{7a}$$

$$\mathbf{M}_{lm}^{(i)}(\mathbf{r}) = \frac{1}{k}\nabla \times \mathbf{N}_{lm}^{(i)}(\mathbf{r}). \tag{7b}$$

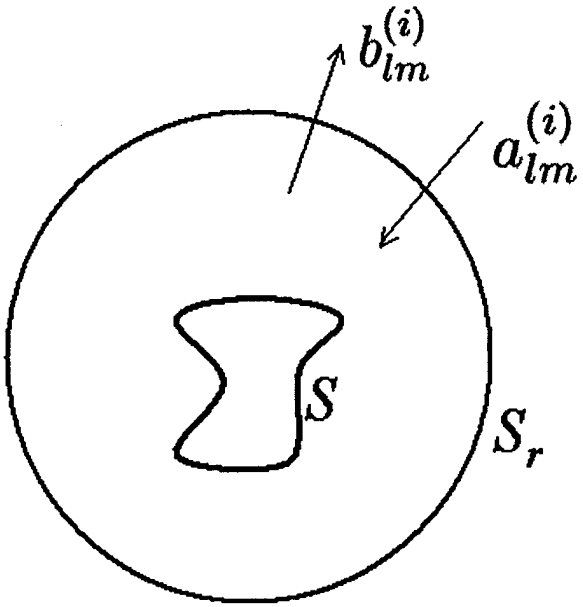

Figure 1: Schematic diagram of the scattering problem.

The $\mathbf{M}_{lm}^{(i)}(\mathbf{r})$ spherical wave functions have no radial component. Because of that the $\mathbf{M}_{lm}^{(i)}(\mathbf{r})$ functions in (5) and the $\mathbf{N}_{lm}^{(i)}(\mathbf{r})$ functions in (6) are often referred to as TE waves while the $\mathbf{N}_{lm}^{(i)}(\mathbf{r})$ functions in (5) and the $\mathbf{M}_{lm}^{(i)}(\mathbf{r})$ functions in (6) are often referred to as TM waves. The $\mathbf{M}_{lm}^{(1)}(\mathbf{r})$ and $\mathbf{N}_{lm}^{(1)}(\mathbf{r})$ functions have the radial dependence $j_l(kr)$ where j_l is the spherical Bessel function of order l and are referred to as "incoming" waves. The $\mathbf{M}_{lm}^{(2)}(\mathbf{r})$ and $\mathbf{N}_{lm}^{(2)}(\mathbf{r})$ functions have the radial dependence $h_l^{(1)}(kr)$ where $h_l^{(1)}$ is the spherical Hankel function of the first kind of order l and are referred to as "outgoing" waves. The expansions in (5) and (6) are known as multipole expansions. The $l = 1$ terms are the dipole terms, the $l = 2$ terms are the quadrupole terms, etc. The summations containing the modal coefficients $a_{lm}^{(i)}$ in (5) and (6) equal the electromagnetic fields produced by the sources that reside outside the surface S_r. The summations containing the modal coefficients $b_{lm}^{(i)}$ in (5) and (6) are the outgoing electromagnetic fields scattered from the surface S.

The "outgoing" modal coefficients $(b_{lm}^{(i)})$ of the scatterer are related to the "incoming" modal coefficients $(a_{lm}^{(i)})$ of the scatterer by a linear matrix transformation termed the "source scattering-matrix equation" [8], [9] for the spherical-wave representation of the scatterer. This source scattering-matrix equation can be written as

$$b_{lm}^{(s)} = \sum_{l'=1}^{\infty} \sum_{m'=-l'}^{l'} \sum_{s'=1}^{2} S_{lm;l'm'}^{(s),(s')} \, a_{l'm'}^{(s')}. \tag{8}$$

The coefficients $S_{lm;l'm'}^{(s),(s')}$ in the source scattering matrix embody the scattering properties of the scatterer.

The spherical-wave source scattering matrix given in (5)–(8) for scatterers differs from the classical spherical-wave scattering-matrix given in [10, secs. 9.18–9.24] because the classical scattering matrix uses $(h_l^{(2)}, h_l^{(1)})$ radial basis functions instead of $(j_l, h_l^{(1)})$. This small mathematical change from $h_l^{(2)}$ to j_l appreciably simplifies the analysis by relating all the scattering-matrix coefficients directly to the physical sources.

3 DIPOLAR SCATTERING FROM LOSSLESS SPHERES

We now specialize our general source scattering-matrix framework to scattering from a lossless penetrable sphere of radius a with relative (to free space) permittivity ϵ_r and relative permeability μ_r. The center of the sphere is assumed located at the origin of a spherical polar coordinate system as shown in Figure 2. The radial dependence of the incoming vector spherical wave functions $\mathbf{M}_{lm}^{(1)}(\mathbf{r})$ is $j_l(kr)$ while that of the incoming wave functions $\mathbf{N}_{lm}^{(1)}(\mathbf{r})$ is $j_l(kr)/(kr)$ for the radial component and $\frac{1}{kr}\frac{\mathrm{d}}{\mathrm{d}(kr)}[(kr)j_l(kr)]$ for the angular components. As $kr \to 0$

$$j_l(kr) \overset{kr \to 0}{\sim} \frac{(kr)^l}{1 \cdot 3 \cdot 5 \cdots (2l+1)} \tag{9a}$$

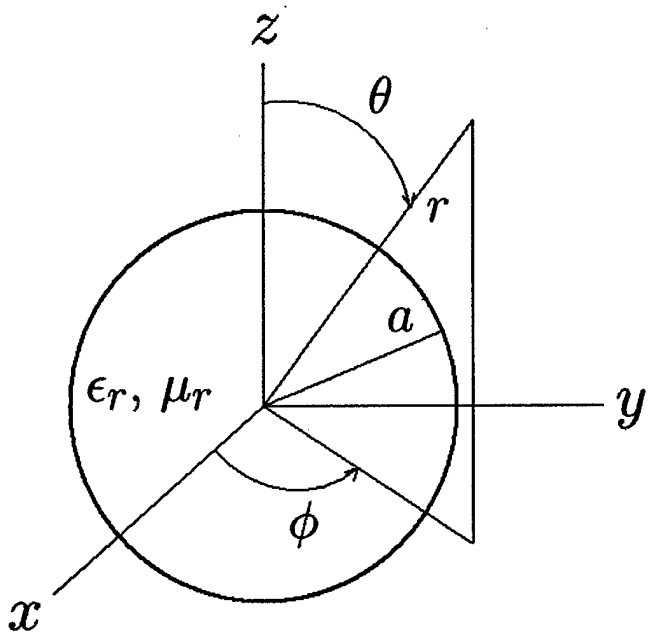

Figure 2: Schematic diagram of a lossless sphere of radius a with relative permittivity ϵ_r and relative permeability μ_r, with center at the origin of a spherical polar coordinate system (r, θ, ϕ).

$$\frac{j_l(kr)}{kr} \overset{kr\to 0}{\sim} \frac{(kr)^{l-1}}{1\cdot 3\cdot 5\cdots(2l+1)} \tag{9b}$$

$$\frac{1}{kr}\frac{\mathrm{d}}{\mathrm{d}(kr)}[(kr)j_l(kr)] \overset{kr\to 0}{\sim} \frac{l+1}{1\cdot 3\cdot 5\cdots(2l+1)}(kr)^{l-1} \tag{9c}$$

so that only the incoming $\mathbf{N}_{1m}^{(1)}(\mathbf{r})$ wave functions are non-zero at the center of the sphere. We assume that either the sphere is sufficiently small that only the dipole scattered fields are excited, or the frequency is such that all the scattered multipole fields are negligible except the dipole fields. Then from the Mie theory of scattering from a sphere [11, sec. 9.25], if the scattered electromagnetic field is that of a magnetic dipole

$$[\mathbf{E}^{sc}, \mathbf{H}^{sc}] = a_1^{sc}[\mathbf{M}_{1m}^{(2)}, -\mathrm{i}Y_0\mathbf{N}_{1m}^{(2)}] \tag{10a}$$

the incident field that excites this magnetic dipole is

$$[\mathbf{E}^{inc}, \mathbf{H}^{inc}] = [\mathbf{M}_{1m}^{(1)}, -\mathrm{i}Y_0\mathbf{N}_{1m}^{(1)}] \tag{10b}$$

while if the scattered electromagnetic field is that of an electric dipole

$$[\mathbf{E}^{sc}, \mathbf{H}^{sc}] = b_1^{sc}[\mathbf{N}_{1m}^{(2)}, -\mathrm{i}Y_0\mathbf{M}_{1m}^{(2)}] \tag{10c}$$

the incident field that excites this electric dipole is

$$[\mathbf{E}^{inc}, \mathbf{H}^{inc}] = [\mathbf{N}_{1m}^{(1)}, -\mathrm{i}Y_0\mathbf{M}_{1m}^{(1)}] \tag{10d}$$

$m = -1, 0, 1$. The Mie dipole scattering coefficients a_1^{sc} and b_1^{sc} in (10a) and (10b) are given by

$$a_1^{sc} = -\frac{\mu_r j_1(\mathrm{m}ka)[(ka)j_1(ka)]' - j_1(ka)[(\mathrm{m}ka)j_1(\mathrm{m}ka)]'}{\mu_r j_1(\mathrm{m}ka)[(ka)h_1^{(1)}(ka)]' - h_1^{(1)}(ka)[(\mathrm{m}ka)j_1(\mathrm{m}ka)]'} \tag{11a}$$

$$b_1^{sc} = -\frac{\mu_r j_1(ka)[(\mathrm{m}ka)j_1(\mathrm{m}ka)]' - \mathrm{m}^2 j_1(\mathrm{m}ka)[(ka)j_1(ka)]'}{\mu_r h_1^{(1)}(ka)[(\mathrm{m}ka)j_1(\mathrm{m}ka)]' - \mathrm{m}^2 j_1(\mathrm{m}ka)[(ka)h_1^{(1)}(ka)]'} \tag{11b}$$

where m is the relative refractive index $\mathrm{m} = \sqrt{\epsilon_r\mu_r}$. Note that the one-to-one relation of the scattered field wave functions to the incoming field wave functions, and hence the restriction of the relevant spherical wave functions to those with $l = 1$ and the same values of the index m as those of the assumed scattered dipole fields, is a consequence of our considering scattering by a homogeneous sphere. Homogeneity can be replaced with radial symmetry and the same conclusion holds. If, however, we were to consider a scatterer of non-spherical shape, or for that matter a penetrable sphere with a non-radial variation of permittivity or permeability, then even if the only scattered electromagnetic field were that, say, of (10a), the exciting incident field would no longer be limited to (10b) and would in general include higher-order wave functions as well. (Conversely, for these asymmetric scatterers, an incident dipole field of the form (10b) or (10d) can excite higher-order multipole fields in addition to the dipole fields of (10a) and (10c).)

Useful properties of the Mie coefficients are [12, sec. 10.21]

$$a_1^{sc} = -\frac{1}{2}\left(1 - \mathrm{e}^{-2\mathrm{i}\alpha_1}\right) \tag{12a}$$

$$|a_1^{sc}|^2 = \sin^2\alpha_1 \tag{12b}$$

$$\tan\alpha_1 = -\frac{\mu_r j_1(\mathrm{m}ka)[(ka)j_1(ka)]' - j_1(ka)[(\mathrm{m}ka)j_1(\mathrm{m}ka)]'}{\mu_r j_1(\mathrm{m}ka)[(ka)y_1(ka)]' - y_1(ka)[(\mathrm{m}ka)j_1(\mathrm{m}ka)]'} \tag{12c}$$

$$\sin\left(\arg[a_1^{sc}] - \frac{\pi}{2}\right) = |a_1^{sc}| \tag{12d}$$

$$\arg[a_1^{sc}] = \tan^{-1}\left[\frac{\sin 2\alpha_1}{-2\sin^2\alpha_1}\right] \tag{12e}$$

and

$$b_1^{sc} = -\frac{1}{2}\left(1 - \mathrm{e}^{-2\mathrm{i}\beta_1}\right) \tag{13a}$$

$$|b_1^{sc}|^2 = \sin^2\beta_1 \tag{13b}$$

$$\tan\beta_1 = -\frac{\mu_r j_1(ka)[(\mathrm{m}ka)j_1(\mathrm{m}ka)]' - \mathrm{m}^2 j_1(\mathrm{m}ka)[(ka)j_1(ka)]'}{\mu_r y_1(ka)[(\mathrm{m}ka)j_1(\mathrm{m}ka)]' - \mathrm{m}^2 j_1(\mathrm{m}ka)[(ka)y_1(ka)]'} \tag{13c}$$

$$\sin\left(\arg[b_1^{sc}] - \frac{\pi}{2}\right) = |b_1^{sc}| \tag{13d}$$

$$\arg[b_1^{sc}] = \tan^{-1}\left[\frac{\sin 2\beta_1}{-2\sin^2\beta_1}\right]. \tag{13e}$$

In (12c) and (13c), $y_1(z)$ is the spherical Neumann function. Similar relationships hold for all the Mie coefficients of lossless scatterers [12, sec. 10.21].[1] Note that the magnitude of the Mie scattering coefficients is at most equal to one. The values of ka for which the magnitude of the Mie coefficients a_1^{sc} and b_1^{sc} equals one correspond to resonances of the free magnetic or electric dipole oscillations of the sphere, respectively [11, sec. 9.25]. As examples of these resonances, in Figures 3, 4, and 5 we show plots of the magnitudes of the Mie dipole coefficients a_1^{sc} and b_1^{sc} for a sphere with $\epsilon_r = 10, \mu_r = 10$, a sphere with $\epsilon_r = 40, \mu_r = 1$, and a sphere with $\epsilon_r = 10, \mu_r = 1$, respectively. (The Mie electric and magnetic coefficients for a sphere with equal relative permittivity and permeability are identical.) In our treatment below of traveling waves on a linear periodic array of spheres, the resonances of the Mie coefficients will play an important role since it is only when the spheres are close to a resonance that there is sufficient scattering from the spheres to support a traveling wave.

Let us now assume that at the center of the sphere the incoming electric and magnetic fields are polarized in the x and y directions, respectively. Then the incoming electromagnetic field can be represented as a linear combination of the fields [see (22a) and (22b)]

$$[\mathbf{E}_1^{inc}, \mathbf{H}_1^{inc}] = \left[\mathbf{M}_{1,-1}^{(1)}(\mathbf{r}) + \mathbf{M}_{1,+1}^{(1)}(\mathbf{r}), -\mathrm{i}Y_0\left(\mathbf{N}_{1,-1}^{(1)}(\mathbf{r}) + \mathbf{N}_{1,+1}^{(1)}(\mathbf{r})\right)\right] \tag{14a}$$

$$[\mathbf{E}_2^{inc}, \mathbf{H}_2^{inc}] = \left[\mathbf{N}_{1,-1}^{(1)}(\mathbf{r}) - \mathbf{N}_{1,+1}^{(1)}(\mathbf{r}), -\mathrm{i}Y_0\left(\mathbf{M}_{1,-1}^{(1)}(\mathbf{r}) - \mathbf{M}_{1,+1}^{(1)}(\mathbf{r})\right)\right]. \tag{14b}$$

---

[1] For scattering from homogeneous lossless spheres, the "outgoing" spherical mode with coefficient $b_{lm}^{(s)}$ in (5)–(6) is excited only by the corresponding "incoming" spherical mode with coefficient $a_{lm}^{(s)}$ in (5)–(6) so that all the $S_{lm;l'm'}^{(s),(s')}$ in (8) are zero except for $(s' = s, l' = l, m' = m)$. The general power conservation relations given in [2, eq. (33)] then reduce to $\mathrm{Re}\left(S_{lm;lm}^{(s),(s)}\right) + \left|S_{lm;lm}^{(s),(s)}\right|^2 = 0$, a relationship that can be rewritten in the form of (12d) and (13d). Also, (5)–(6), (8), and (10) show that $S_{1m;1m}^{(1),(1)} = a_1^{sc}$ and $S_{1m;1m}^{(2),(2)} = b_1^{sc}$, $m = -1, 0, 1$.

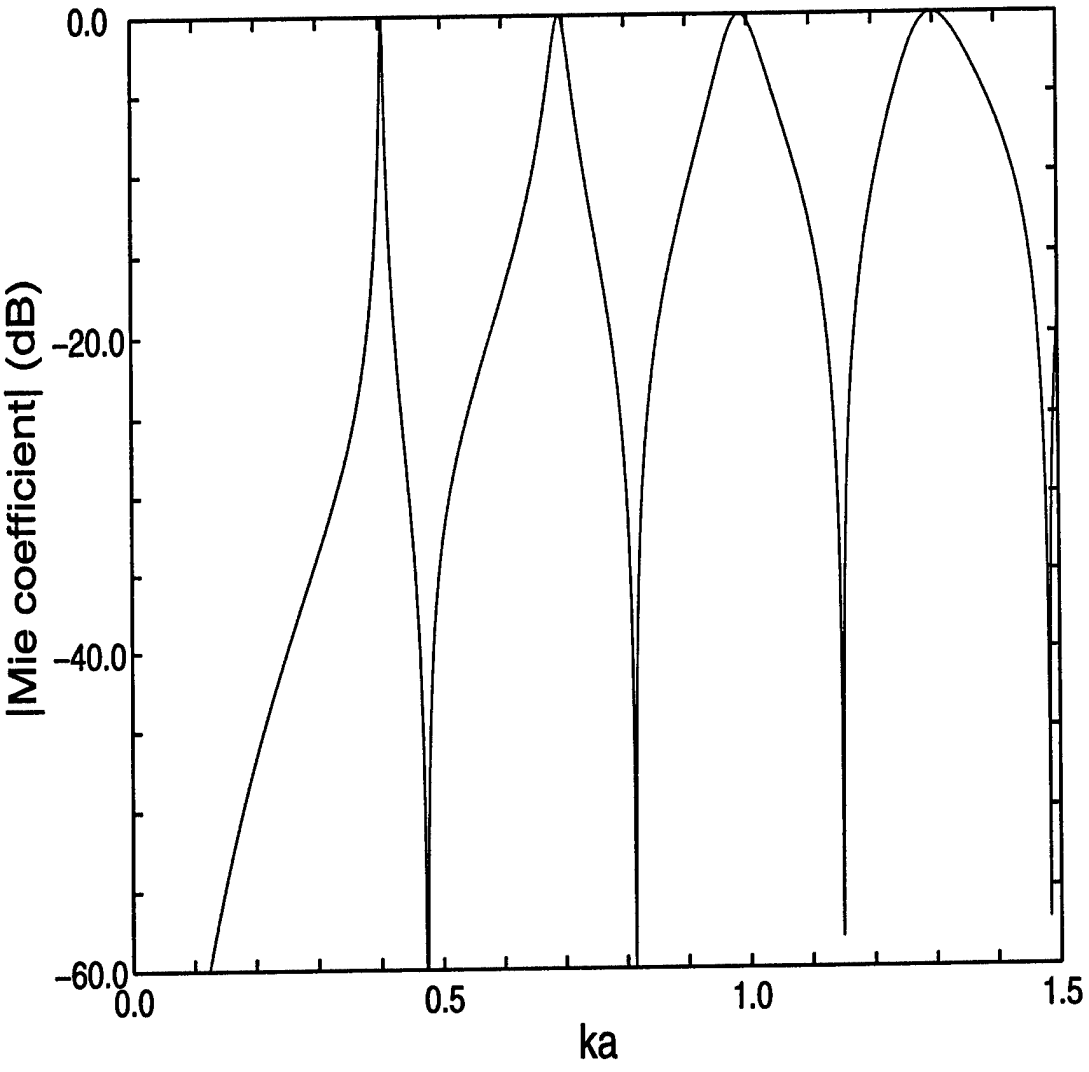

Figure 3: Magnitude of the Mie coefficients a_1^{sc} and b_1^{sc} for a sphere with $\epsilon_r = 10, \mu_r = 10$.

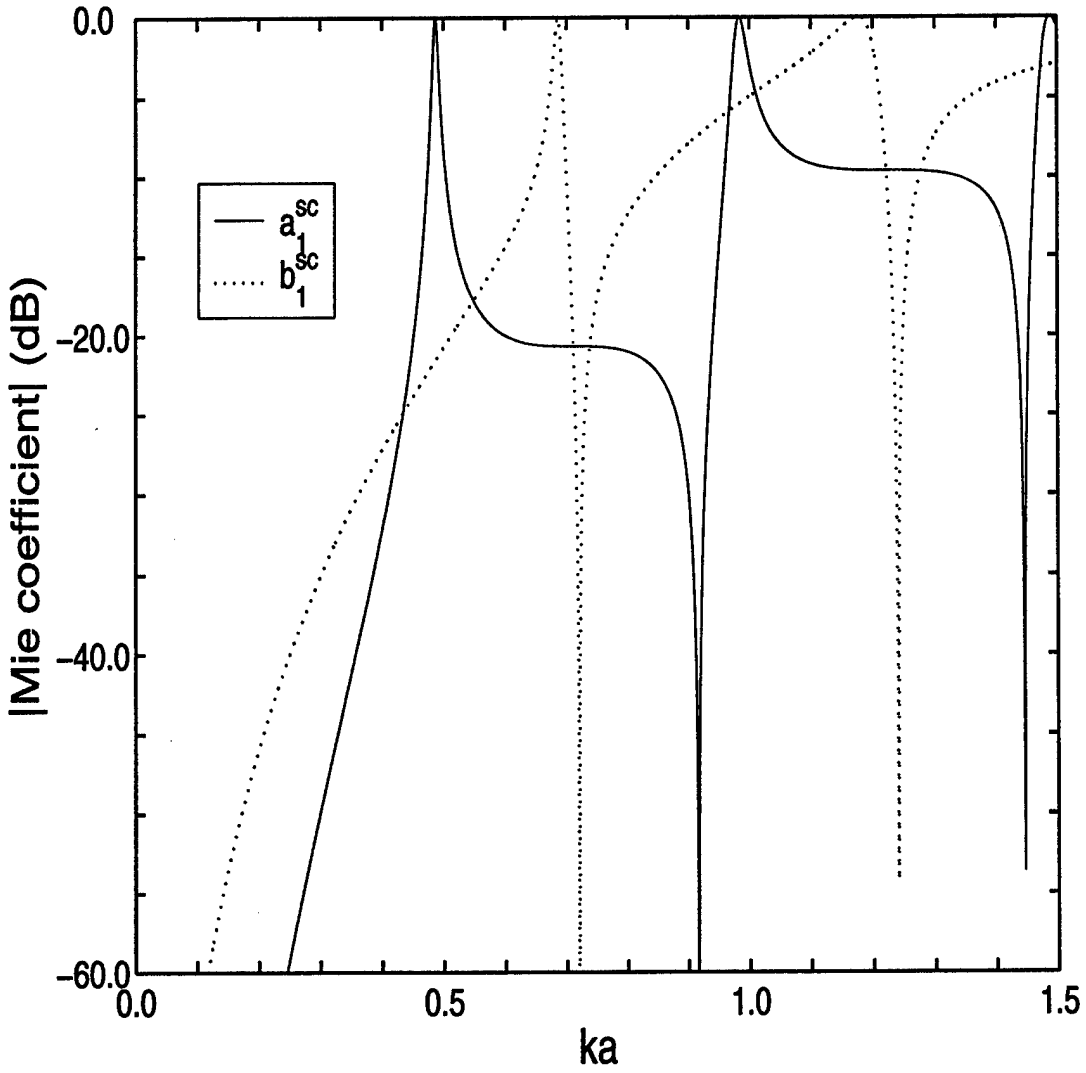

Figure 4: Magnitude of the Mie coefficients a_1^{sc} and b_1^{sc} for a sphere with $\epsilon_r = 40, \mu_r = 1$.

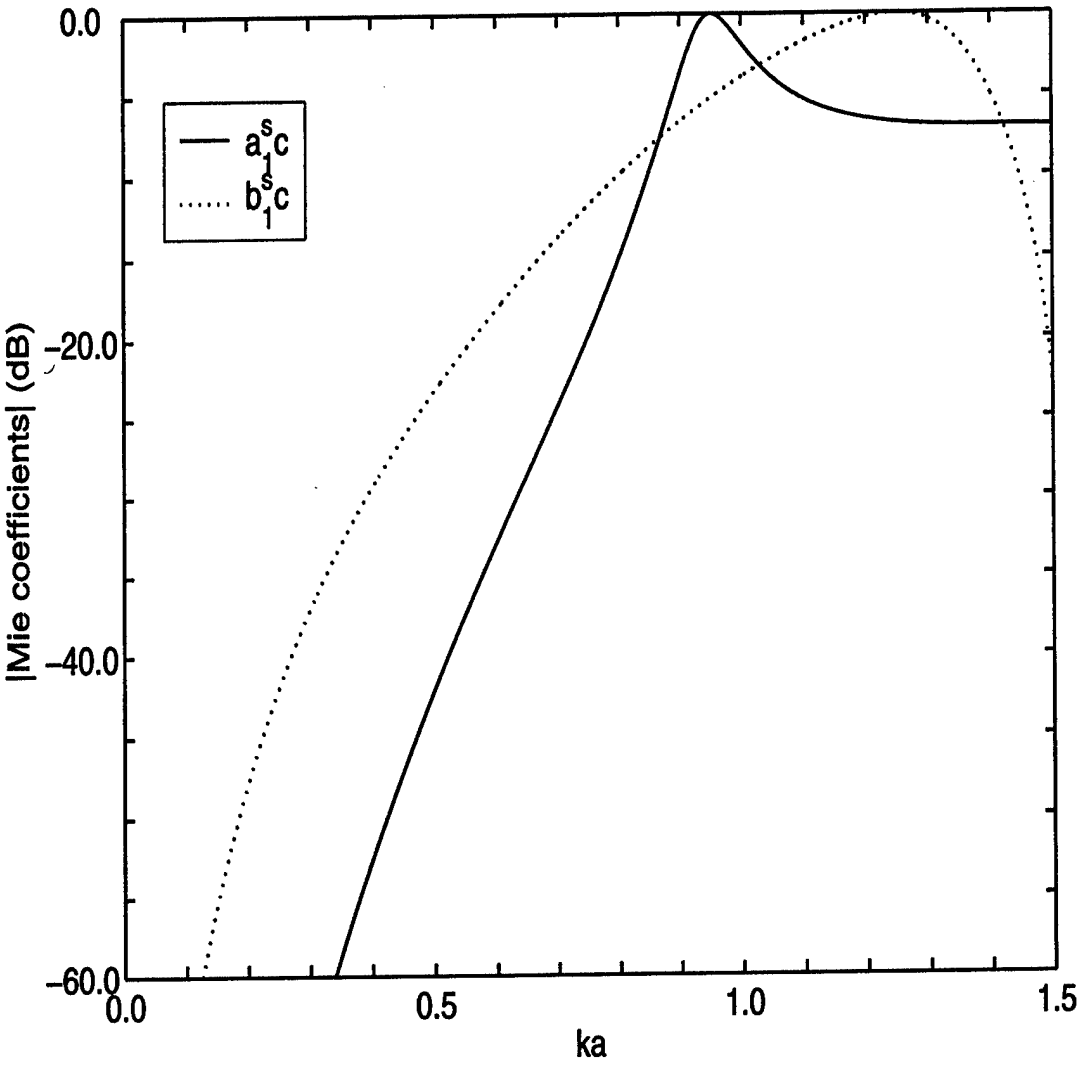

Figure 5: Magnitude of the Mie coefficients a_1^{sc} and b_1^{sc} for a sphere with $\epsilon_r = 10, \mu_r = 1$.

The corresponding scattered fields are then a linear combination of the fields

$$[\mathbf{E}_1^{sc}, \mathbf{H}_1^{sc}] = \left[\mathbf{M}_{1,-1}^{(2)}(\mathbf{r}) + \mathbf{M}_{1,+1}^{(2)}(\mathbf{r}), -\mathrm{i}Y_0\left(\mathbf{N}_{1,-1}^{(2)}(\mathbf{r}) + \mathbf{N}_{1,+1}^{(2)}(\mathbf{r})\right)\right] \tag{15a}$$

$$[\mathbf{E}_2^{sc}, \mathbf{H}_2^{sc}] = \left[\mathbf{N}_{1,-1}^{(2)}(\mathbf{r}) - \mathbf{N}_{1,+1}^{(2)}(\mathbf{r}), -\mathrm{i}Y_0\left(\mathbf{M}_{1,-1}^{(2)}(\mathbf{r}) - \mathbf{M}_{1,+1}^{(2)}(\mathbf{r})\right)\right]. \tag{15b}$$

Because these fields will play a central role in what follows it is convenient to define a set of "combination modes"

$$\mathbf{N}_{1,-}^{(i)}(\mathbf{r}) = \mathbf{N}_{1,-1}^{(i)}(\mathbf{r}) - \mathbf{N}_{1,+1}^{(i)}(\mathbf{r}), \quad \mathbf{N}_{1,+}^{(i)}(\mathbf{r}) = \mathbf{N}_{1,-1}^{(i)}(\mathbf{r}) + \mathbf{N}_{1,+1}^{(i)}(\mathbf{r}) \tag{16a}$$

$$\mathbf{M}_{1,-}^{(i)}(\mathbf{r}) = \mathbf{M}_{1,-1}^{(i)}(\mathbf{r}) - \mathbf{M}_{1,+1}^{(i)}(\mathbf{r}), \quad \mathbf{M}_{1,+}^{(i)}(\mathbf{r}) = \mathbf{M}_{1,-1}^{(i)}(\mathbf{r}) + \mathbf{M}_{1,+1}^{(i)}(\mathbf{r}) \tag{16b}$$

$i = 1, 2$. These combination modes are directly related to the vector wave functions $\mathbf{n}$ and $\mathbf{m}$ used by Stratton [11, p. 416]:

$$\mathbf{N}_{1,-}^{(i)}(\mathbf{r}) = \frac{\mathrm{i}}{2}\sqrt{\frac{3}{\pi}}\mathbf{n}_{e11}^{(j)}(\mathbf{r}) \tag{17a}$$

$$\mathbf{N}_{1,+}^{(i)}(\mathbf{r}) = \frac{1}{2}\sqrt{\frac{3}{\pi}}\mathbf{n}_{o11}^{(j)}(\mathbf{r}) \tag{17b}$$

$$\mathbf{M}_{1,-}^{(i)}(\mathbf{r}) = \frac{\mathrm{i}}{2}\sqrt{\frac{3}{\pi}}\mathbf{m}_{e11}^{(j)}(\mathbf{r}) \tag{17c}$$

$$\mathbf{M}_{1,+}^{(i)}(\mathbf{r}) = \frac{1}{2}\sqrt{\frac{3}{\pi}}\mathbf{m}_{o11}^{(j)}(\mathbf{r}) \tag{17d}$$

where $(i) = 1 \leftrightarrow (j) = 1$ and $(i) = 2 \leftrightarrow (j) = 3$. Explicit expressions for the outgoing combination modes are as follows:

$$\mathbf{N}_{1,-}^{(2)}(\mathbf{r}) = \sqrt{\frac{3}{\pi}}\frac{\mathrm{e}^{\mathrm{i}kr}}{kr}\left[-\frac{\mathrm{i}}{kr}\left(1 + \frac{\mathrm{i}}{kr}\right)\sin\theta\cos\phi\hat{\mathbf{r}} + \frac{1}{2}\left(1 + \frac{\mathrm{i}}{kr} - \frac{1}{(kr)^2}\right)(\cos\theta\cos\phi\hat{\boldsymbol{\theta}} - \sin\phi\hat{\boldsymbol{\phi}})\right] \tag{18a}$$

$$\mathbf{N}_{1,+}^{(2)}(\mathbf{r}) = -\sqrt{\frac{3}{\pi}}\frac{\mathrm{e}^{\mathrm{i}kr}}{kr}\left[\frac{1}{kr}\left(1 + \frac{i}{kr}\right)\sin\theta\sin\phi\hat{\mathbf{r}} + \frac{i}{2}\left(1 + \frac{i}{kr} - \frac{1}{(kr)^2}\right)(\cos\theta\sin\phi\hat{\boldsymbol{\theta}} + \cos\phi\hat{\boldsymbol{\phi}})\right] \tag{18b}$$

$$\mathbf{M}_{1,-}^{(2)}(\mathbf{r}) = \frac{i}{2}\sqrt{\frac{3}{\pi}}\frac{\mathrm{e}^{\mathrm{i}kr}}{kr}\left(1 + \frac{\mathrm{i}}{kr}\right)(\sin\phi\hat{\boldsymbol{\theta}} + \cos\theta\cos\phi\hat{\boldsymbol{\phi}}) \tag{18c}$$

$$\mathbf{M}_{1,+}^{(2)}(\mathbf{r}) = -\frac{1}{2}\sqrt{\frac{3}{\pi}}\frac{\mathrm{e}^{\mathrm{i}kr}}{kr}\left(1 + \frac{\mathrm{i}}{kr}\right)(\cos\phi\hat{\boldsymbol{\theta}} - \cos\theta\sin\phi\hat{\boldsymbol{\phi}}). \tag{18d}$$

The scattered electromagnetic fields of (15a) and (15b), now written as

$$[\mathbf{E}_1^{sc}, \mathbf{H}_1^{sc}] = \left[\mathbf{M}_{1,+}^{(2)}(\mathbf{r}), -\mathrm{i}Y_0\mathbf{N}_{1,+}^{(2)}(\mathbf{r})\right] \tag{19a}$$

and

$$[\mathbf{E}_2^{sc}, \mathbf{H}_2^{sc}] = \left[\mathbf{N}_{1,-}^{(2)}(\mathbf{r}), -\mathrm{i}Y_0\mathbf{M}_{1,-}^{(2)}(\mathbf{r})\right] \tag{19b}$$

are proportional to the fields radiated by an infinitesimal y directed magnetic dipole and x directed electric dipole respectively.

Explicit expressions for the incoming combination modes are

$$\mathbf{N}_{1,-}^{(1)}(\mathbf{r}) = \mathrm{i}\sqrt{\frac{3}{\pi}}\left[\frac{j_1(kr)}{kr}\sin\theta\cos\phi\hat{\mathbf{r}} + \frac{1}{2}\frac{1}{kr}\frac{\mathrm{d}}{\mathrm{d}(kr)}\left(\cos\theta\cos\phi\hat{\boldsymbol{\theta}} - \sin\phi\hat{\boldsymbol{\phi}}\right)\right] \tag{20a}$$

$$\mathbf{N}_{1,+}^{(1)}(\mathbf{r}) = \sqrt{\frac{3}{\pi}}\left[\frac{j_1(kr)}{kr}\sin\theta\sin\phi\hat{\mathbf{r}} + \frac{1}{2}\frac{1}{kr}\frac{\mathrm{d}}{\mathrm{d}(kr)}\left(\cos\theta\sin\phi\hat{\boldsymbol{\theta}} + \cos\phi\hat{\boldsymbol{\phi}}\right)\right] \tag{20b}$$

$$\mathbf{M}_{1,-}^{(1)}(\mathbf{r}) = -\mathrm{i}\frac{1}{2}\sqrt{\frac{3}{\pi}}j_1(kr)\left(\sin\phi\hat{\boldsymbol{\theta}} + \cos\theta\cos\phi\hat{\boldsymbol{\phi}}\right) \tag{20c}$$

$$\mathbf{M}_{1,+}^{(1)}(\mathbf{r}) = \frac{1}{2}\sqrt{\frac{3}{\pi}}j_1(kr)\left(\cos\phi\hat{\boldsymbol{\theta}} - \cos\theta\sin\phi\hat{\boldsymbol{\phi}}\right) \tag{20d}$$

where

$$j_1(z) = \frac{\sin z}{z^2} - \frac{\cos z}{z} \tag{21a}$$

$$\frac{j_1(z)}{z} = \frac{\sin z}{z^3} - \frac{\cos z}{z^2} \tag{21b}$$

and

$$\frac{1}{z}\frac{\mathrm{d}}{\mathrm{d}z}\left[zj_1(z)\right] = \frac{\cos z}{z^2} + \frac{\sin z}{z}\left(1 - \frac{1}{z^2}\right). \tag{21c}$$

Limiting expressions for the incoming combination modes as $kr \to 0$ are

$$\mathbf{N}_{1,-}^{(1)}(\mathbf{r}) \overset{kr\to 0}{\longrightarrow} \frac{\mathrm{i}}{3}\sqrt{\frac{3}{\pi}}\hat{\mathbf{x}} \tag{22a}$$

$$\mathbf{N}_{1,+}^{(1)}(\mathbf{r}) \overset{kr\to 0}{\longrightarrow} \frac{1}{3}\sqrt{\frac{3}{\pi}}\hat{\mathbf{y}} \tag{22b}$$

and

$$\mathbf{M}_{1,\pm}^{(1)}(\mathbf{r}) \overset{kr\to 0}{=} O(kr). \tag{22c}$$

From the Mie theory of scattering from a sphere (10a)-(10d), the source scattering-matrix equations for the combination modes can be written as

$$b_{1,+}^{(1)} = S_{1,+;1,+}^{(1),(1)}\, a_{1,+}^{(1)} \tag{23a}$$

$$b_{1,-}^{(2)} = S_{1,-;1,-}^{(2),(2)}\, a_{1,-}^{(2)} \tag{23b}$$

where $a_{1,+}^{(1)}$ is the coefficient of the incoming electromagnetic field $[\mathbf{M}_{1,+}^{(1)}(\mathbf{r}), -\mathrm{i}Y_0\mathbf{N}_{1,+}^{(1)}(\mathbf{r})]$, $b_{1,+}^{(1)}$ is the coefficient of the corresponding outgoing electromagnetic field $[\mathbf{M}_{1,+}^{(2)}(\mathbf{r}), -\mathrm{i}Y_0\mathbf{M}_{1,+}^{(2)}(\mathbf{r})]$, $a_{1,-}^{(2)}$ is the coefficient of the incoming electromagnetic field $[\mathbf{N}_{1,-}^{(1)}(\mathbf{r}), -\mathrm{i}Y_0\mathbf{M}_{1,-}^{(1)}(\mathbf{r})]$, $b_{1,-}^{(2)}$ is the coefficient of the corresponding outgoing electromagnetic field $[\mathbf{N}_{1,-}^{(2)}(\mathbf{r}), -\mathrm{i}Y_0\mathbf{M}_{1,-}^{(2)}(\mathbf{r})]$,

and the scattering coefficients $S^{(1),(1)}_{1,+;1,+}$ and $S^{(2),(2)}_{1,-;1,-}$ are equal to the Mie coefficients given by (11a) and (11b)

$$S^{(1),(1)}_{1,+;1,+} = a_1^{sc} \tag{24a}$$

$$S^{(2),(2)}_{1,-;1,-} = b_1^{sc}. \tag{24b}$$

Note from Footnote 1 that $S^{(1),(1)}_{1,+;1,+} = S^{(1),(1)}_{1m;1m}$ and $S^{(2),(2)}_{1,-;1,-} = S^{(2),(2)}_{1m;1m}$, $m = \pm 1$.

It will be convenient to normalize the scattering-matrix equations. As $r \to 0$ the incoming electric field $\mathbf{E}^0(\mathbf{r}) = a^{(2)}_{1,-}\mathbf{N}^{(1)}_{1,-}(\mathbf{r})$ reduces to

$$\mathbf{E}^0(\mathbf{r}) \overset{r\to 0}{\sim} a^{(2)}_{1,-}\frac{\mathrm{i}}{\sqrt{3\pi}}\hat{\mathbf{x}} \tag{25a}$$

and the incoming magnetic field $\mathbf{H}^0(\mathbf{r}) = a^{(1)}_{1,+}(-\mathrm{i}Y_0)\mathbf{N}^{(1)}_{1,+}(\mathbf{r})$ reduces to

$$\mathbf{H}^0(\mathbf{r}) \overset{r\to 0}{\sim} a^{(1)}_{1,+}(-\mathrm{i}Y_0)\frac{1}{\sqrt{3\pi}}\hat{\mathbf{y}}. \tag{25b}$$

The incident electric and magnetic dipole spherical waves are the only multipoles with nonzero fields at the center of the sphere ($r = 0$). Let

$$E^0_x = a^{(2)}_{1,-}\frac{\mathrm{i}}{\sqrt{3\pi}}, \quad H^0_y = a^{(1)}_{1,+}(-\mathrm{i}Y_0)\frac{1}{\sqrt{3\pi}}. \tag{26}$$

Then

$$a^{(2)}_{1,-} = \frac{E^0_x}{\dfrac{\mathrm{i}}{\sqrt{3\pi}}}, \quad a^{(2)}_{1,+} = \frac{H^0_y}{Y_0\dfrac{-\mathrm{i}}{\sqrt{3\pi}}} \tag{27}$$

Now let b_- be the coefficient of $\dfrac{\mathrm{e}^{ikr}}{kr}$ in the transverse component of the outgoing electric field $b^{(2)}_{1,-}\mathbf{N}^{(2)}_{1,-}(\mathbf{r})$ [see (18a)] and b_+ be the coefficient of $\dfrac{\mathrm{e}^{ikr}}{kr}$ in the outgoing electric field $b^{(1)}_{1,+}\mathbf{M}^{(2)}_{1,+}(\mathbf{r})$ [see (18d)] so that

$$b_- = b^{(2)}_{1,-}\frac{1}{2}\sqrt{\frac{3}{\pi}} \tag{28a}$$

$$b_+ = -b^{(1)}_{1,+}\frac{1}{2}\sqrt{\frac{3}{\pi}}. \tag{28b}$$

Then the scattering matrix equations (23a) and (23b) become

$$b_- = -\mathrm{i}\frac{3}{2}\,S^{(2),(2)}_{1,-;1,-}\,E^0_x \tag{29a}$$

$$b_+ = -\mathrm{i}\frac{3}{2}\,S^{(1),(1)}_{1,+;1,+}\,\frac{H^0_y}{Y_0}. \tag{29b}$$

Finally, normalize the scattering coefficients by letting

$$S_- = -\mathrm{i}\frac{3}{2}\,S^{(2),(2)}_{1,-;1,-} = -\mathrm{i}\frac{3}{2}\,b_1^{sc} \tag{30a}$$

$$S_+ = -\mathrm{i}\frac{3}{2}\, S^{(1),(1)}_{1,+;1,+} = -\mathrm{i}\frac{3}{2}\, a_1^{sc}. \tag{30b}$$

Then the normalized form of the scattering matrix equations is simply

$$b_- = S_-\, E_x^0 \tag{31a}$$

$$b_+ = S_+\, \frac{H_y^0}{Y_0}. \tag{31b}$$

Since these equations form the basis of our treatment of dipolar traveling waves on an infinite linear periodic array of penetrable spheres it is worthwhile to elucidate their meaning. Equation (31a) says that if the electric field incident on a penetrable sphere has the value $E_x^0\,\hat{\mathbf{x}}$ at $r = 0$, then the corresponding scattered electric and magnetic dipole fields are [see (18a) and (18c)]

$$\mathbf{E}^{sc} = b_-\frac{\mathrm{e}^{\mathrm{i}kr}}{kr}\left[-2\frac{\mathrm{i}}{kr}\left(1+\frac{\mathrm{i}}{kr}\right)\sin\theta\cos\phi\hat{\mathbf{r}} + \left(1+\frac{\mathrm{i}}{kr}-\frac{1}{(kr)^2}\right)(\cos\theta\cos\phi\hat{\boldsymbol{\theta}} - \sin\phi\hat{\boldsymbol{\phi}})\right] \tag{32a}$$

$$\mathbf{H}^{sc} = Y_0 b_-\frac{\mathrm{e}^{\mathrm{i}kr}}{kr}\left(1+\frac{\mathrm{i}}{kr}\right)(\sin\phi\hat{\boldsymbol{\theta}} + \cos\theta\cos\phi\hat{\boldsymbol{\phi}}). \tag{32b}$$

Equation (31b) says that if the magnetic field incident on a penetrable sphere has the value $H_y^0\,\hat{\mathbf{y}}$ at $r = 0$, then the corresponding scattered electric and magnetic dipole fields are [see (18d) and (18b)]

$$\mathbf{E}^{sc} = b_+\frac{\mathrm{e}^{\mathrm{i}kr}}{kr}\left(1+\frac{\mathrm{i}}{kr}\right)(\cos\phi\hat{\boldsymbol{\theta}} - \cos\theta\sin\phi\hat{\boldsymbol{\phi}}) \tag{33a}$$

$$\mathbf{H}^{sc} = -iY_0 b_+\frac{\mathrm{e}^{\mathrm{i}kr}}{kr}\left[\frac{2}{kr}\left(1+\frac{i}{kr}\right)\sin\theta\sin\phi\hat{\mathbf{r}} + \mathrm{i}\left(1+\frac{\mathrm{i}}{kr}-\frac{1}{(kr)^2}\right)(\cos\theta\sin\phi\hat{\boldsymbol{\theta}} + \cos\phi\hat{\boldsymbol{\phi}})\right]. \tag{33b}$$

The scattered fields in (32) and (33) are those of an x directed electric dipole and y directed magnetic dipole, respectively. In treating on-axis scattering from an infinite linear periodic array of penetrable spheres in the next section it will be useful to have expressions for the special cases of equations (32) and (33) when $\theta = 0$ and $\theta = \pi$, that is, on the axis of the array. From the standard expressions relating the unit vectors in spherical polar and cartesian coordinates we obtain from (32)

$$\mathbf{E}^{sc} = b_-\frac{\mathrm{e}^{\mathrm{i}kr}}{kr}\left(1+\frac{\mathrm{i}}{kr}-\frac{1}{(kr)^2}\right)\hat{\mathbf{x}},\ \theta = 0,\pi \tag{34a}$$

$$\mathbf{H}^{sc} = \pm Y_0 b_-\frac{\mathrm{e}^{\mathrm{i}kr}}{kr}\left(1+\frac{\mathrm{i}}{kr}\right)\hat{\mathbf{y}},\ \theta = 0,\pi \tag{34b}$$

and from (33) we obtain

$$\mathbf{E}^{sc} = \pm b_+\frac{\mathrm{e}^{\mathrm{i}kr}}{kr}\left(1+\frac{\mathrm{i}}{kr}\right)\hat{\mathbf{x}},\ \theta = 0,\pi \tag{35a}$$

$$\mathbf{H}^{sc} = Y_0 b_+\frac{\mathrm{e}^{\mathrm{i}kr}}{kr}\left(1+\frac{\mathrm{i}}{kr}-\frac{1}{(kr)^2}\right)\hat{\mathbf{y}},\ \theta = 0,\pi. \tag{35b}$$

4 ON-AXIS DIPOLAR SCATTERING EQUATIONS FOR AN INFINITE LINEAR PERIODIC ARRAY OF LOSSLESS PENETRABLE SPHERES

The on-axis dipole scattering-matrix equations for a infinite linear periodic array of lossless penetrable spheres with radius a, relative permittivity ϵ_r and relative permeability μ_r can now be easily obtained. These equations are the basis for the treatment of dipolar traveling waves on an infinite linear periodic array of lossless penetrable spheres given in Section 5. We denote the separation between the centers of adjacent spheres by d, take the z axis to be the axis of the array, and assume an excitation of the array with an x directed electric field and a y directed magnetic field (see Figure 6). The x directed electric field at the center of the nth sphere resulting from the electric fields scattered by all the other spheres in the array is then, from (34a) and (35a),

$$E_x^{0n} = \sum_{\substack{j=-\infty \\ j\neq n}}^{\infty} b_{-,j} \frac{e^{ikd|j-n|}}{kd|j-n|}\left(1+\frac{i}{kd|j-n|}-\frac{1}{(kd)^2|j-n|^2}\right)$$

$$+\sum_{j=-\infty}^{n-1} b_{+,j}\frac{e^{ikd(n-j)}}{kd(n-j)}\left(1+\frac{i}{kd(n-j)}\right)-\sum_{j=n+1}^{\infty} b_{+,j}\frac{e^{ikd(j-n)}}{kd(j-n)}\left(1+\frac{i}{kd(j-n)}\right). \quad (36)$$

Since $b_{-,n} = S_- E_x^{0n}$

$$b_{-,n} = S_-\Big[\sum_{\substack{j=-\infty \\ j\neq n}}^{\infty} b_{-,j} \frac{e^{ikd|j-n|}}{kd|j-n|}\left(1+\frac{i}{kd|j-n|}-\frac{1}{(kd)^2|j-n|^2}\right)$$

$$+\sum_{j=-\infty}^{n-1} b_{+,j}\frac{e^{ikd(n-j)}}{kd(n-j)}\left(1+\frac{i}{kd(n-j)}\right)-\sum_{j=n+1}^{\infty} b_{+,j}\frac{e^{ikd(j-n)}}{kd(j-n)}\left(1+\frac{i}{kd(j-n)}\right)\Big]. \quad (37)$$

Similarly the y directed magnetic field at the center of the nth sphere resulting from the magnetic fields scattered by all the other spheres in the array is, from (34b) and (35b),

$$\frac{H_y^{0n}}{Y_0} = \sum_{\substack{j=-\infty \\ j\neq n}}^{\infty} b_{+,j} \frac{e^{ikd|j-n|}}{kd|j-n|}\left(1+\frac{i}{kd|j-n|}-\frac{1}{(kd)^2|j-n|^2}\right)$$

$$+\sum_{j=-\infty}^{n-1} b_{-,j}\frac{e^{ikd(n-j)}}{kd(n-j)}\left(1+\frac{i}{kd(n-j)}\right)-\sum_{j=n+1}^{\infty} b_{-,j}\frac{e^{ikd(j-n)}}{kd(j-n)}\left(1+\frac{i}{kd(j-n)}\right). \quad (38)$$

Since $b_{+,n} = S_+ \dfrac{H_y^{0n}}{Y_0}$

$$b_{+,n} = S_+\Big[\sum_{\substack{j=-\infty \\ j\neq n}}^{\infty} b_{+,j} \frac{e^{ikd|j-n|}}{kd|j-n|}\left(1+\frac{i}{kd|j-n|}-\frac{1}{(kd)^2|j-n|^2}\right)$$

$$+\sum_{j=-\infty}^{n-1} b_{-,j}\frac{e^{ikd(n-j)}}{kd(n-j)}\left(1+\frac{i}{kd(n-j)}\right)-\sum_{j=n+1}^{\infty} b_{-,j}\frac{e^{ikd(j-n)}}{kd(j-n)}\left(1+\frac{i}{kd(j-n)}\right)\Big]. \quad (39)$$

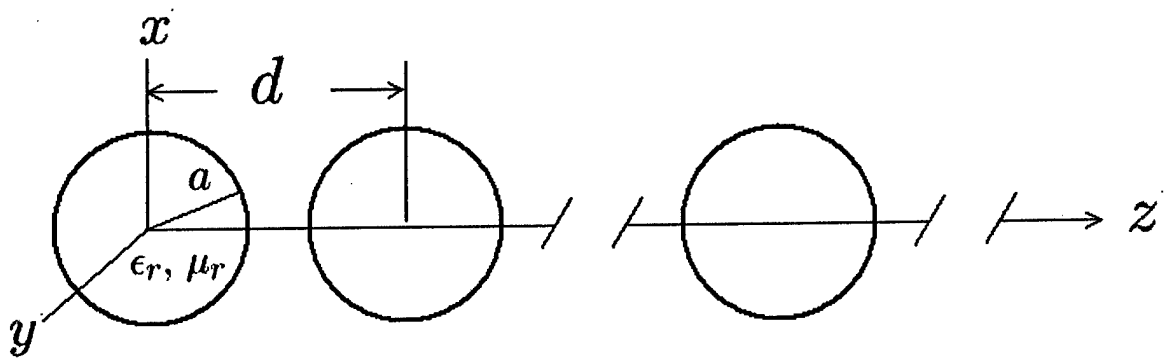

Figure 6: Schematic diagram of an infinite linear periodic array of lossless, penetrable spheres of radius a with relative permittivity ϵ_r, relative permeability μ_r, and separation distance d.

5 DIPOLAR TRAVELING WAVES ON AN INFINITE LINEAR PERIODIC ARRAY OF LOSSLESS PENETRABLE SPHERES

We now come to the central objective of this report — the derivation of an expression for the propagation constant of a dipolar traveling wave supported by an infinite linear periodic array of lossless penetrable spheres. If the array supports a dipolar traveling wave with a real propagation constant β to be determined, then the $b_{-,j}$ in (37) and (39) are identical except for a phase shift given by

$$b_{-,j} = b_{-,0}\mathrm{e}^{\mathrm{i}\beta jd}, \quad 0 < \beta d < \pi \tag{40a}$$

and similarly

$$b_{+,j} = b_{+,0}\mathrm{e}^{\mathrm{i}\beta jd}, \quad 0 < \beta d < \pi. \tag{40b}$$

This allows (37) and (39) to be written as

$$\begin{aligned} 1 = S_-\Bigg\{ &\sum_{\substack{j=-\infty \\ j\neq n}}^{\infty} \mathrm{e}^{\mathrm{i}\beta d(j-n)} \frac{\mathrm{e}^{\mathrm{i}kd|j-n|}}{kd|j-n|}\left(1 + \frac{\mathrm{i}}{kd|j-n|} - \frac{1}{(kd)^2|j-n|^2}\right) \\ &+ \frac{b_{0,+}}{b_{0,-}}\Bigg[\sum_{j=-\infty}^{n-1} \mathrm{e}^{\mathrm{i}\beta d(j-n)} \frac{\mathrm{e}^{\mathrm{i}kd(n-j)}}{kd(n-j)}\left(1 + \frac{\mathrm{i}}{kd(n-j)}\right) \\ &- \sum_{j=n+1}^{\infty} \mathrm{e}^{\mathrm{i}\beta d(j-n)} \frac{\mathrm{e}^{\mathrm{i}kd(j-n)}}{kd(j-n)}\left(1 + \frac{\mathrm{i}}{kd(j-n)}\right)\Bigg]\Bigg\}, \quad n = 0, \pm 1, \pm 2, \cdots \end{aligned} \tag{41}$$

and

$$\begin{aligned} 1 = S_+\Bigg\{ &\sum_{\substack{j=-\infty \\ j\neq n}}^{\infty} \mathrm{e}^{\mathrm{i}\beta d(j-n)} \frac{\mathrm{e}^{\mathrm{i}kd|j-n|}}{kd|j-n|}\left(1 + \frac{\mathrm{i}}{kd|j-n|} - \frac{1}{(kd)^2|j-n|^2}\right) \\ &+ \frac{b_{0,-}}{b_{0,+}}\Bigg[\sum_{j=-\infty}^{n-1} \mathrm{e}^{\mathrm{i}\beta d(j-n)} \frac{\mathrm{e}^{\mathrm{i}kd(n-j)}}{kd(n-j)}\left(1 + \frac{\mathrm{i}}{kd(n-j)}\right) \\ &- \sum_{j=n+1}^{\infty} \mathrm{e}^{\mathrm{i}\beta d(j-n)} \frac{\mathrm{e}^{\mathrm{i}kd(j-n)}}{kd(j-n)}\left(1 + \frac{\mathrm{i}}{kd(j-n)}\right)\Bigg]\Bigg\}, \quad n = 0, \pm 1, \pm 2, \cdots . \end{aligned} \tag{42}$$

Since the values of the summations are independent of the value of n, we can set $n = 0$. Multiplying by $(kd)^3$ we then obtain the equations

$$\begin{aligned} (kd)^3 = S_-\Bigg[&\sum_{j=1}^{\infty}\left(\frac{\mathrm{e}^{\mathrm{i}(k+\beta)dj} + \mathrm{e}^{-\mathrm{i}(\beta-k)dj}}{j}\right)\left((kd)^2 + \frac{\mathrm{i}kd}{j} - \frac{1}{j^2}\right) \\ &+ \frac{b_{0,+}}{b_{0,-}}(kd)\sum_{j=1}^{\infty}\left(\frac{\mathrm{e}^{\mathrm{i}(k+\beta)dj} - \mathrm{e}^{-\mathrm{i}(\beta-k)dj}}{j}\right)\left(kd + \frac{\mathrm{i}}{j}\right)\Bigg] \end{aligned} \tag{43}$$

and

$$(kd)^3 = S_+\Bigg[\sum_{j=1}^{\infty}\left(\frac{\mathrm{e}^{\mathrm{i}(k+\beta)dj} + \mathrm{e}^{-\mathrm{i}(\beta-k)dj}}{j}\right)\left((kd)^2 + \frac{\mathrm{i}kd}{j} - \frac{1}{j^2}\right)$$

$$+\frac{b_{0,-}}{b_{0,+}}(kd)\sum_{j=1}^{\infty}\left(\frac{e^{i(k+\beta)dj}-e^{-i(\beta-k)dj}}{j}\right)\left(kd+\frac{i}{j}\right)\Bigg] \tag{44}$$

Now let

$$p=\frac{b_{0,+}}{b_{0,-}}. \tag{45}$$

(Recall — see (23a, 23b), (15a, 15b), and (40a, 40b) — that the electromagnetic field scattered from each of the spheres in the array is, apart from the phase factor of the traveling wave, a linear combination of an electromagnetic field proportional to the field of an infinitesimal x directed electric dipole with a normalized coefficient $b_{-,0}$, and an electromagnetic field proportional to the field of an infinitesimal y directed magnetic dipole with normalized coefficient $b_{+,0}$, so that p is the ratio of these two normalized scattered field coefficients.) Also let

$$\Sigma_1=\sum_{j=1}^{\infty}\left(\frac{e^{i(k+\beta)dj}+e^{-i(\beta-k)dj}}{j}\right)\left((kd)^2+\frac{ikd}{j}-\frac{1}{j^2}\right) \tag{46a}$$

and

$$\Sigma_2=kd\sum_{j=1}^{\infty}\left(\frac{e^{i(k+\beta)dj}-e^{-i(\beta-k)dj}}{j}\right)\left(kd+\frac{i}{j}\right). \tag{46b}$$

Using the summation formulas [13, sec. 1.441, eqs. 1 and 2; sec. 1.443, eqs. 3 and 5]

$$\sum_{j=1}^{\infty}\frac{\cos ja}{j}=\frac{1}{2}\ln\frac{1}{2(1-\cos a)}=-\ln\left[2\sin(a/2)\right],\quad 0<a<2\pi \tag{47a}$$

$$\sum_{j=1}^{\infty}\frac{\sin ja}{j}=\frac{\pi-a}{2},\quad 0<a<2\pi \tag{47b}$$

$$\sum_{j=1}^{\infty}\frac{\cos ja}{j^2}=\frac{\pi^2}{6}-\frac{\pi a}{2}+\frac{a^2}{4},\quad 0<a<2\pi \tag{47c}$$

$$\sum_{j=1}^{\infty}\frac{\sin ja}{j^3}=\frac{\pi^2 a}{6}-\frac{\pi a^2}{4}+\frac{a^3}{12},\quad 0<a<2\pi \tag{47d}$$

and the approximations (see Appendix B)

$$\sum_{j=1}^{\infty}\frac{\sin ja}{j^2}\equiv F(a)\approx -0.1381\sin a+0.03212\sin 2a-0.9653a\ln(a/\pi),\quad 0<a<\pi \tag{48a}$$

$$F(a)=-F(2\pi-a),\quad \pi\le a<2\pi \tag{48b}$$

and

$$\sum_{j=1}^{\infty}\frac{\cos ja}{j^3}\equiv G(a)\approx 1.3328-0.1424\cos a+0.01094\cos 2a+0.4902a^2\ln(a/\pi)-0.2417a^2,\quad 0<a<\pi \tag{48c}$$

$$G(a)=G(2\pi-a),\quad \pi\le a<2\pi \tag{48d}$$

the summations Σ_1 and Σ_2 can be expressed in closed form as

$$\Sigma_1 = -(kd)^2 \ln\left[2\left(\cos kd - \cos\beta d\right)\right] - (kd)\left[F(kd+\beta d) - F(\beta d - kd)\right]$$
$$- \left[G(kd+\beta d) + G(\beta d - kd)\right] - \mathrm{i}\frac{2}{3}(kd)^3 \tag{49}$$

and

$$\Sigma_2 = -(kd)^2\left[\ln\sin\left(\frac{kd+\beta d}{2}\right) - \ln\sin\left(\frac{\beta d - kd}{2}\right)\right] - (kd)\left[F(kd+\beta d) + F(\beta d - kd)\right]. \tag{50}$$

The on-axis scattering equations (43) and (44) can then be written as

$$(kd)^3 = S_-\left(\Sigma_1 + p\Sigma_2\right) \tag{51a}$$

and

$$(kd)^3 = S_+\left(\Sigma_1 + \frac{1}{p}\Sigma_2\right). \tag{51b}$$

Equations (51a, 51b) are a pair of simultaneous equations determining the two unknowns p and βd. We can solve for p in each of these two equations and equate the resulting expressions, thus obtaining

$$\frac{(kd)^3 - S_-\Sigma_1}{S_-\Sigma_2} = \frac{S_+\Sigma_2}{(kd)^3 - S_+\Sigma_1}. \tag{52}$$

It is important to note that the quantity p given by either side of (52) is real. For, using the expression for p given by the LHS of (52), the fact that the imaginary part of Σ_1 is $-\frac{2}{3}(kd)^3$ [see (49)] and that Σ_2 is real [see (50)], the definition of S_- in (30a), and the property (13d) of the Mie coefficient b_1^{sc} it follows that

$$\Sigma_2\,\mathrm{Im}[p] = (kd)^3\,\mathrm{Im}\left[\frac{1}{S_-}\right] - \mathrm{Im}[\Sigma_1] = (kd)^3\left(\mathrm{Im}\left[\frac{1}{S_-}\right] + \frac{2}{3}\right) = 0. \tag{53}$$

The same conclusion can be obtained similarly from considering the RHS of (52). Equation (52) can then be easily solved numerically for βd given kd.

It is worth noting as a check on the consistency of what we have done that if we divide (51a) by S_- and then let $S_- = |S_-|\exp(\mathrm{i}\psi_-)$ and equate real and imaginary parts with p real, we obtain

$$-\frac{(kd)^3}{|S_-|}\sin\psi_- = -\frac{2}{3}(kd)^3 \tag{54}$$

or

$$|S_-| = \frac{3}{2}\sin\psi_-\,, \tag{55}$$

a result that is consistent with (30a) and (13d). A similar check can be performed with (51b) to produce $|S_+| = (3/2)\sin\psi_+$. We note that (55) is identical with the equation obtained for the magnitude of the effective scattering coefficient of a small, reciprocal, lossless electric

dipole in [2]. As a further check on the validity of (52), we note that when S_+, the normalized magnetic dipole scattering coefficient, is equal to zero, then (52) reduces to

$$(kd)^3 - S_-\Sigma_1 = 0. \tag{56}$$

This equation is identical to equation (72) of [2] that determines the $k - \beta$ diagram for the traveling waves on a linear array of electric dipoles perpendicular to the array axis.

It is easy to show that if βd is a solution of (52) then so is $2\pi - \beta d$ (Σ_1 is unchanged and Σ_2 is reversed in sign if $2\pi - \beta d$ is substituted for βd) . The significance of this is that if one had a fast wave, for example, $\pi < \beta d < 2\pi$ then, as shown in general by Yaghjian [1], β' with $0 < \beta' d = 2\pi - \beta d < \pi$ is the propagation constant of a slow traveling wave in the negative z direction, $\exp(-\mathrm{i}\beta' z)$. Therefore, it is unnecessary to consider values of βd greater than π in the $kd - \beta d$ diagrams of traveling waves.

6 COATED SPHERES

The analysis that has been performed in the previous three sections has assumed that the relative permittivity and permeability of the spheres is constant throughout the entire sphere. The analysis, however, carries over almost identically if the relative permittivity and permeability of the spheres is allowed to vary from one spherical shell to another. As one of the simplest examples, assume that the relative permittivity and permeability of each sphere is equal to ϵ_{r1} and μ_{r1}, respectively, for $0 \le \rho < a$, and is equal to ϵ_{r2} and μ_{r2}, respectively, for $a < \rho \le b$ where b is the radius of the sphere. Let m_1 and m_2 be the relative refractive indices $\mathrm{m}_1 = \sqrt{\epsilon_{r1}\mu_{r1}}$ and $\mathrm{m}_2 = \sqrt{\epsilon_{r2}\mu_{r2}}$, respectively, for the two regions of the sphere. Then [14, sect. 8.1] the scattering coefficients of the coated sphere, a_{1c}^{sc} and b_{1c}^{sc}, analogous to the Mie coefficients a_1^{sc} and b_1^{sc} for the homogeneous sphere given by (11a) and (11b) are as follows:

$$a_{1c}^{sc} = -\frac{j_1(\rho_2)\left\{[\mathrm{m}_2\rho_2 j_1(\mathrm{m}_2\rho_2)]' + A\,[\mathrm{m}_2\rho_2 y_1(\mathrm{m}_2\rho_2)]'\right\} - \mu_{2r}\,[\rho_2 j_1(\rho_2)]'\,[j_1(\mathrm{m}_2\rho_2) + A y_n(\mathrm{m}_2\rho_2)]}{h_1^{(1)}(\rho_2)\left\{[\mathrm{m}_2\rho_2 j_1(\mathrm{m}_2\rho_2)]' + A\,[\mathrm{m}_2\rho_2 y_1(\mathrm{m}_2\rho_2)]'\right\} - \mu_{2r}\left[\rho_2 h_1^{(1)}(\rho_2)\right]'\,[j_1(\mathrm{m}_2\rho_2) + A y_n(\mathrm{m}_2\rho_2)]} \tag{57}$$

$$b_{1c}^{sc} = -\frac{\mu_{r2} j_1(\rho_2)\left\{[\mathrm{m}_2\rho_2 j_1(\mathrm{m}_2\rho_2)]' + B\,[\mathrm{m}_2\rho_2 y_1(\mathrm{m}_2\rho_2)]'\right\} - \mathrm{m}_2^2\,[\rho_2 j_1(\rho_2)]'\,[j_1(\mathrm{m}_2\rho_2) + B y_n(\mathrm{m}_2\rho_2)]}{\mu_{r2} h_1^{(1)}(\rho_2)\left\{[\mathrm{m}_2\rho_2 j_1(\mathrm{m}_2\rho_2)]' + B\,[\mathrm{m}_2\rho_2 y_1(\mathrm{m}_2\rho_2)]'\right\} - \mathrm{m}_2^2\left[\rho_2 h_1^{(1)}(\rho_2)\right]'\,[j_1(\mathrm{m}_2\rho_2) + B y_n(\mathrm{m}_2\rho_2)]} \tag{58}$$

where $\rho_1 = ka$, $\rho_2 = kb$, and

$$A = -\frac{\mu_{r1} j_1(\mathrm{m}_1\rho_1)[(\mathrm{m}_2\rho_1) j_1(\mathrm{m}_2\rho_1]' - \mu_{r2} j_1(\mathrm{m}_2\rho_1)[\mathrm{m}_1\rho_1 j_1(\mathrm{m}_1\rho_1)]'}{\mu_{r1} j_1(\mathrm{m}_1\rho_1)[(\mathrm{m}_2\rho_1) y_1(\mathrm{m}_2\rho_1)]' - \mu_{r2} y_1(\mathrm{m}_2\rho_1)[(\mathrm{m}_1\rho_1) j_1(\mathrm{m}_1\rho_1)]'} \tag{59}$$

$$B = -\frac{\mu_{r1}\mathrm{m}_2^2 j_1(\mathrm{m}_2\rho_1)[(\mathrm{m}_1\rho_1) j_1(\mathrm{m}_1\rho_1)]' - \mu_{r2}\mathrm{m}_1^2 j_1(\mathrm{m}_1\rho_1)[(\mathrm{m}_2\rho_1) j_1(\mathrm{m}_2\rho_1)]'}{\mu_{r1}\mathrm{m}_2^2 y_1(\mathrm{m}_2\rho_1)[(\mathrm{m}_1\rho_1) j_1(\mathrm{m}_1\rho_1)]' - \mu_{r2}\mathrm{m}_1^2 j_1(\mathrm{m}_1\rho_1)[(\mathrm{m}_2\rho_1) y_1(\mathrm{m}_2\rho_1)]'}\,. \tag{60}$$

The equations corresponding to (12a-12e) and (13a-13e) are as follows:

$$a_{1c}^{sc} = -\frac{1}{2}\left(1 - \mathrm{e}^{-2\mathrm{i}\alpha_{1c}}\right) \tag{61a}$$

$$|a_{1c}^{sc}|^2 = \sin^2 \alpha_{1c} \tag{61b}$$

$$\tan \alpha_{1c} = -\frac{\mu_{2r}\mathcal{A}a' - a\mathcal{A}'}{\mu_{2r}\mathcal{A}c' - c\mathcal{A}'} \tag{61c}$$

$$\sin\left(\arg\left[a_{1c}^{sc}\right] - \frac{\pi}{2}\right) = |a_{1c}^{sc}| \tag{61d}$$

$$\arg\left[a_{1c}^{sc}\right] = \tan^{-1}\left[\frac{\sin 2\alpha_{1c}}{-2\sin^2 \alpha_{1c}}\right] \tag{61e}$$

and

$$b_{1c}^{sc} = -\frac{1}{2}\left(1 - \mathrm{e}^{-2\mathrm{i}\beta_{1c}}\right) \tag{62a}$$

$$|b_{1c}^{sc}|^2 = \sin^2 \beta_{1c} \tag{62b}$$

$$\tan \beta_{1c} = -\frac{\mu_{2r}\mathcal{B}'a - \mathrm{m}_2^2\mathcal{B}a'}{\mu_{2r}\mathcal{B}'c - \mathrm{m}_2^2\mathcal{B}c'} \tag{62c}$$

$$\sin\left(\arg\left[b_{1c}^{sc}\right] - \frac{\pi}{2}\right) = |b_{1c}^{sc}| \tag{62d}$$

$$\arg\left[b_{1c}^{sc}\right] = \tan^{-1}\left[\frac{\sin 2\beta_{1c}}{-2\sin^2 \beta_{1c}}\right] \tag{62e}$$

where

$$\mathcal{A} = j_1(\mathrm{m}_2\rho_2) + Ay_1(\mathrm{m}_2\rho_2) \tag{63a}$$

$$\mathcal{A}' = [(\mathrm{m}_2\rho_2)j_1(\mathrm{m}_2\rho_2)]' + A[(\mathrm{m}_2\rho_2)y_1(\mathrm{m}_2\rho_2)]' \tag{63b}$$

$$a = j_1(\rho_2) \tag{63c}$$

$$a' = [\rho_2 j_1(\rho_2]' \tag{63d}$$

$$c = y_1(\rho_2) \tag{63e}$$

$$c' = [\rho_2 y_1(\rho_2) \tag{63f}$$

$$\mathcal{B} = j_1(\mathrm{m}_2\rho_2) + By_1(\mathrm{m}_2\rho_2) \tag{63g}$$

and

$$\mathcal{B}' = [(\mathrm{m}_2\rho_2)j_1(\mathrm{m}_2\rho_2)]' + B[(\mathrm{m}_2\rho_2)y_1(\mathrm{m}_2\rho_2)]' \,. \tag{63h}$$

The central result of Section 5, equation (52) that implicitly gives the propagation constant of a dipolar traveling wave on an array of homogeneous spheres in terms of the free-space wave number and the normalized scattering coefficients of the spheres, then holds for coated spheres as well if b_{1c}^{r} and a_{1c}^{r} are substituted for b_1^{sc} and a_1^{sc}, respectively, in (30a) and (30b).

7 NUMERICAL RESULTS

Computer calculations have been performed to illustrate the theory of dipolar traveling waves on linear periodic arrays of lossless spheres that we have presented. The computations fall into two main categories. In the first set of calculations the electrical radius of the spheres, ka, is held constant and the electrical inter-sphere separation distance, kd, is varied to obtain βd where β is the propagation constant of the traveling wave. In the second set of computations the ratio of the sphere radius to the inter-sphere separation distance, a/d, is held constant, and kd is varied to obtain βd. In both sets of calculations we present the $kd - \beta d$ diagram showing a plot of kd versus βd. The second set of calculations corresponds to a laboratory measurement procedure in which frequency is varied and so is much more practicable than the first set which corresponds to a fixed frequency in a laboratory measurement procedure.

To begin with we show some $kd - \beta d$ diagrams for a linear periodic array of spheres with $\epsilon_r = \mu_r = 10$ for ka equal to several different resonances of the Mie scattering coefficients. Figure 7 shows the $kd - \beta d$ diagrams for $ka = 0.405, 0.693$, and 0.998. The smallest value of kd in these diagrams must, of course, be greater than $2ka$, otherwise the spheres will overlap. We observe that the curves end when $\beta d = kd$, that is, when the traveling wave propagation constant β equals the free-space wavenumber k. The importance of having ka equal to, or close to, a resonance of the Mie coefficients a_1^{sc} and b_1^{sc} ($a_1^{sc} = b_1^{sc}$ when $\epsilon_r = \mu_r$) is intuitively clear since a traveling wave with β significantly greater than k cannot be excited without a high degree of scattering coupling between the spheres composing the array. For small values of the scattering coefficients such coupling cannot exist. Traveling waves with $\beta \gg k$ on a linear periodic array of lossless spheres thus exist only within a fairly narrow ka "window".

Next in Figure 8 we show the $kd - \beta d$ diagram for a linear periodic array of spheres with $\epsilon_r = 40, \mu_r = 1$ and $ka = 0.480$, very close to the resonance of the a_1^{sc} Mie coefficient at $ka = 0.487$. The shape of the $kd - \beta d$ diagram is somewhat the reverse of the $kd - \beta d$ diagram of Figure 7 for $\epsilon_r = 10, \mu_r = 10$, and $ka = 0.405$. In Figure 9 we show a detail of Figure 8 for the region of $1.060 < kd \leq 1.100$. What is particularly interesting here is the region for $1.060 < kd < 1.082$ where there are two values of the traveling wave propagation constant for each inter-sphere separation distance.

Figure 10 demonstrates the remarkable sensitivity of the $kd - \beta d$ diagram of Figure 8 to the size of the spheres. As ka increases only the small amount from 0.480 to 0.4844 the $kd - \beta d$ diagram shrinks to a small curve in the vicinity of $\beta d = 3.0, kd = 1.8$. For $ka = 0.4845$ no traveling wave can be supported by the linear array of spheres.

Another example of the possibility of there being two different traveling waves that can be supported by the same linear array of lossless spheres is shown in the $kd - \beta d$ diagram of Figure 11 for $\epsilon_r = 10, \mu_r = 1$, and $ka = 1.1$. (The value of $ka = 1.1$ is approximately halfway between the resonance of the Mie scattering coefficient a_1^{sc} at 0.951 and the resonance of b_1^{sc} at 1.251 .) For $2.337 < kd < 2.346$ there are two values of βd corresponding to each value of the electrical inter-sphere separation distance kd.

We now turn to the second group of calculations, those for which the ratio of the sphere radius to the inter-sphere separation distance, a/d, is held constant, and kd is varied to obtain βd. As noted above, these calculations correspond to the practical laboratory measurement procedure of setting up an array of spheres and then investigating the behavior of traveling waves on the array as the frequency is varied. Figure 12 shows the $kd - \beta d$ diagram obtained

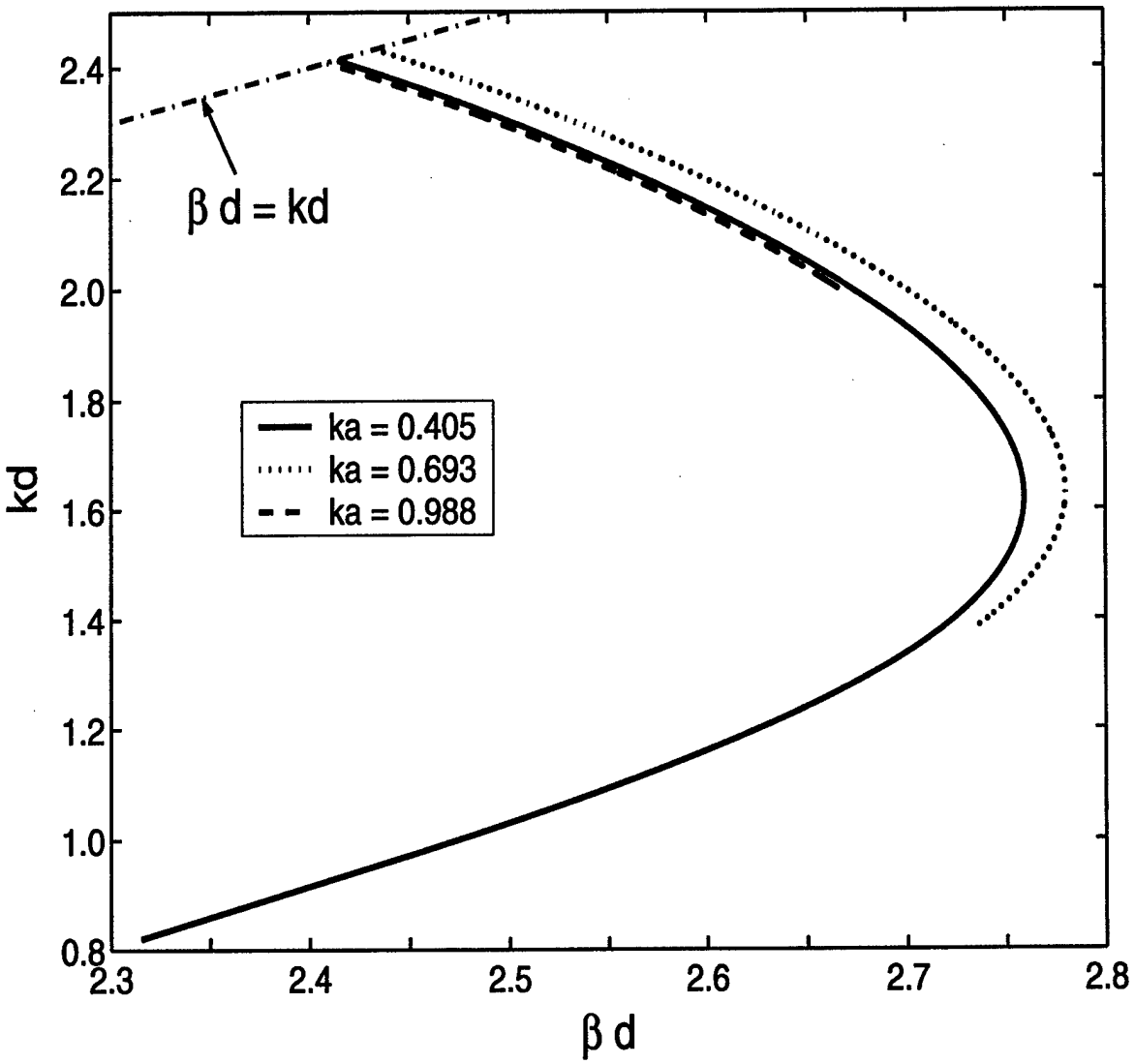

Figure 7: kd — βd diagrams for traveling waves on an infinite linear periodic array of lossless, penetrable spheres, $\epsilon_r = 10$, $\mu_r = 10$.

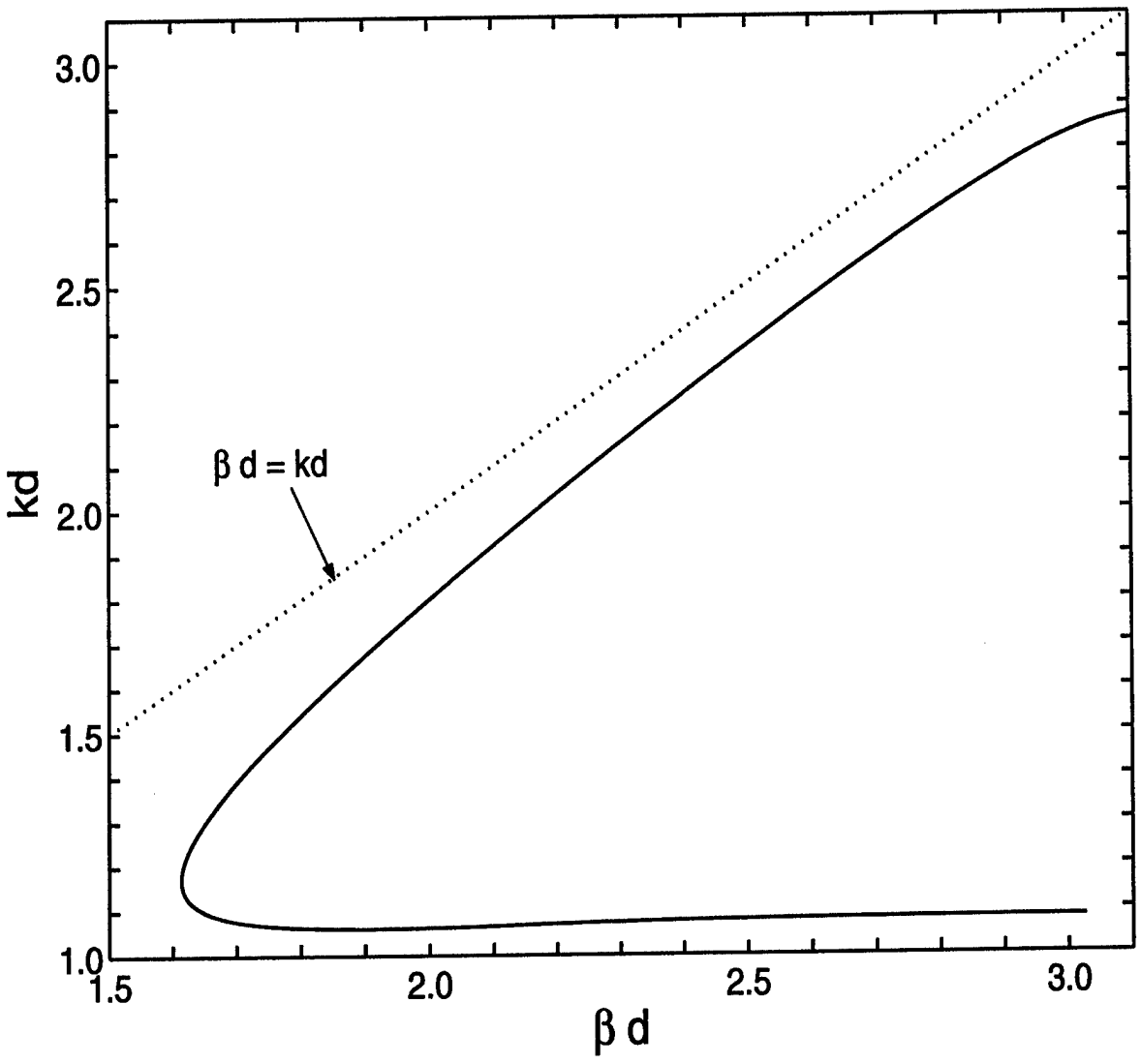

Figure 8: kd — βd diagram for a traveling wave on an infinite linear periodic array of spheres with $\epsilon_r = 40, \mu_r = 1$, and $ka = 0.480$.

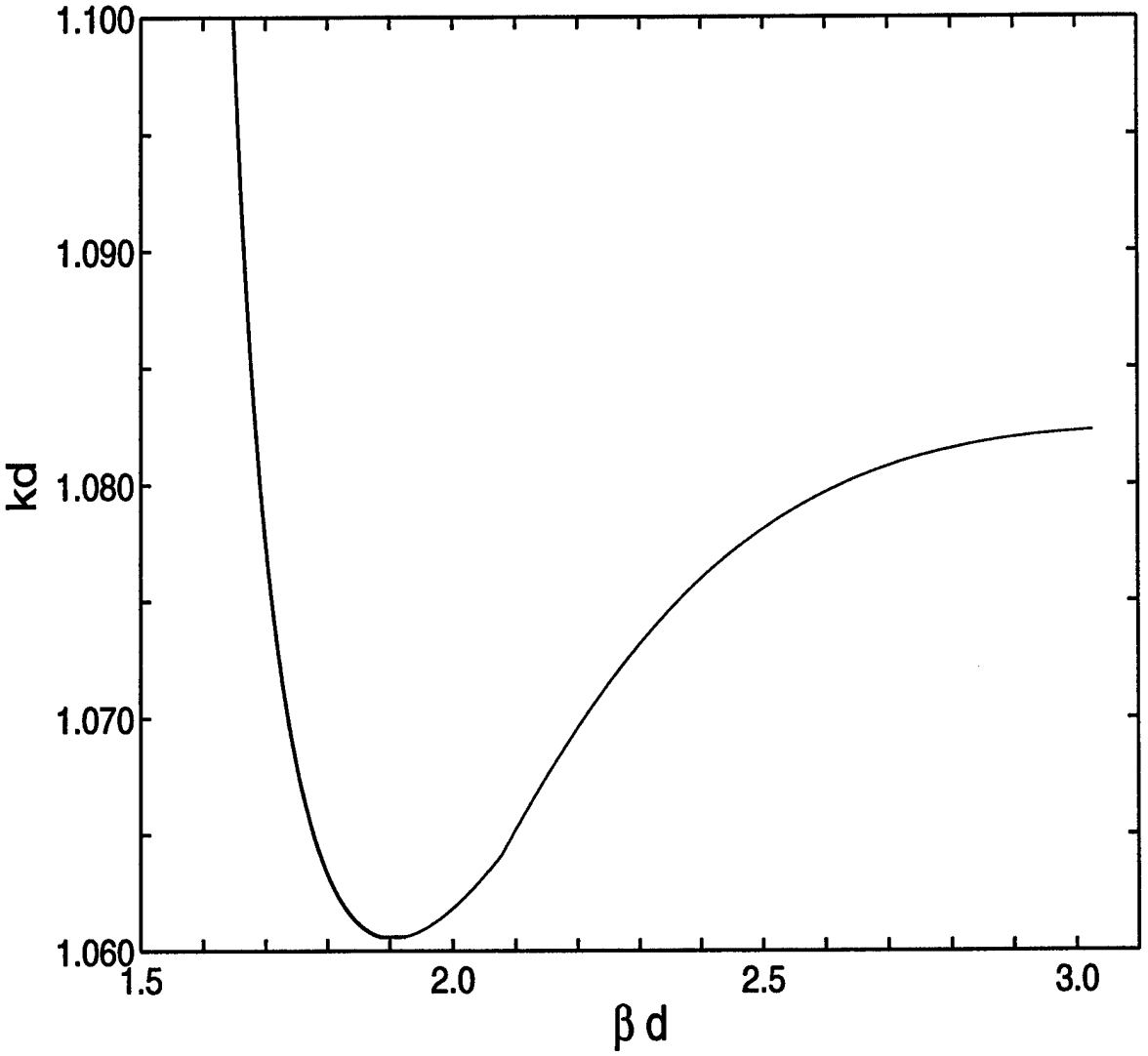

Figure 9: kd — βd diagram for a traveling wave on an infinite linear periodic array of spheres with $\epsilon_r = 40, \mu_r = 1$, and $ka = 0.480$; detail of Figure 8.

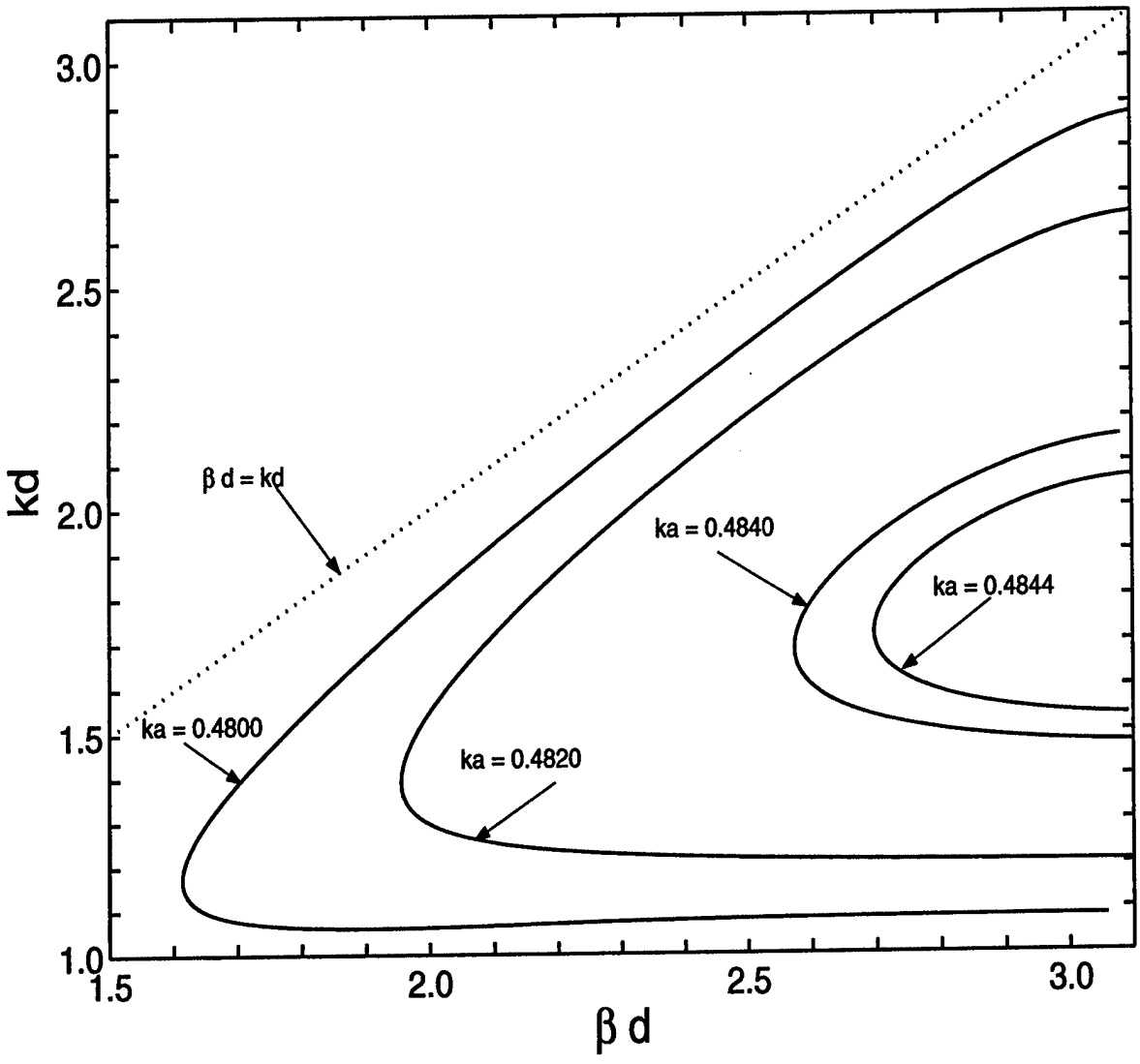

Figure 10: Sensitivity of kd — βd diagrams for traveling waves on an infinite linear periodic array of spheres with $\epsilon_r = 40, \mu_r = 1$, and ka varying from 0.4800 to 0.4844.

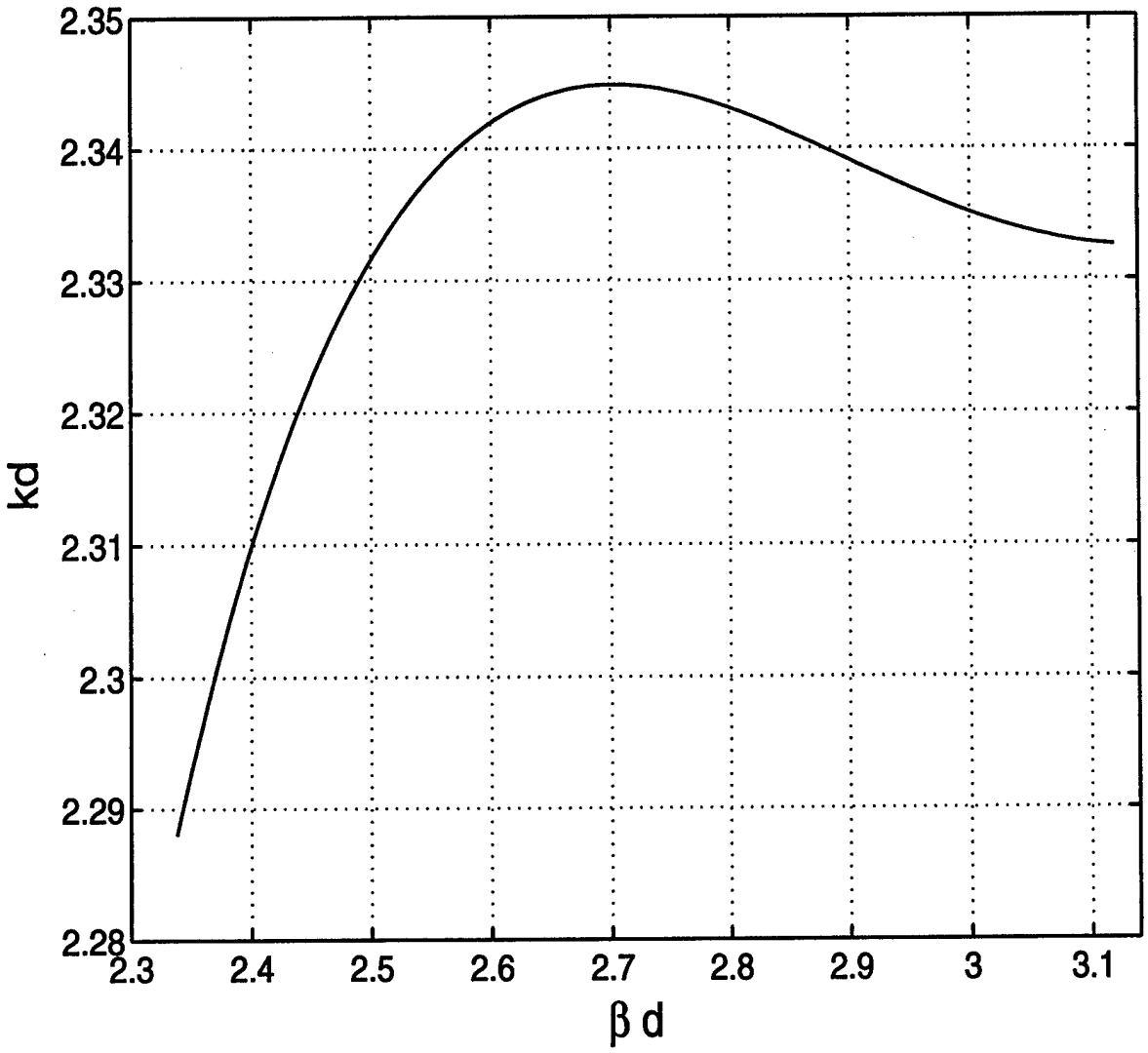

Figure 11: kd — βd diagram for a traveling wave on an infinite linear periodic array of spheres with $\epsilon_r = 10, \mu_r = 1$, and $ka = 1.1$.

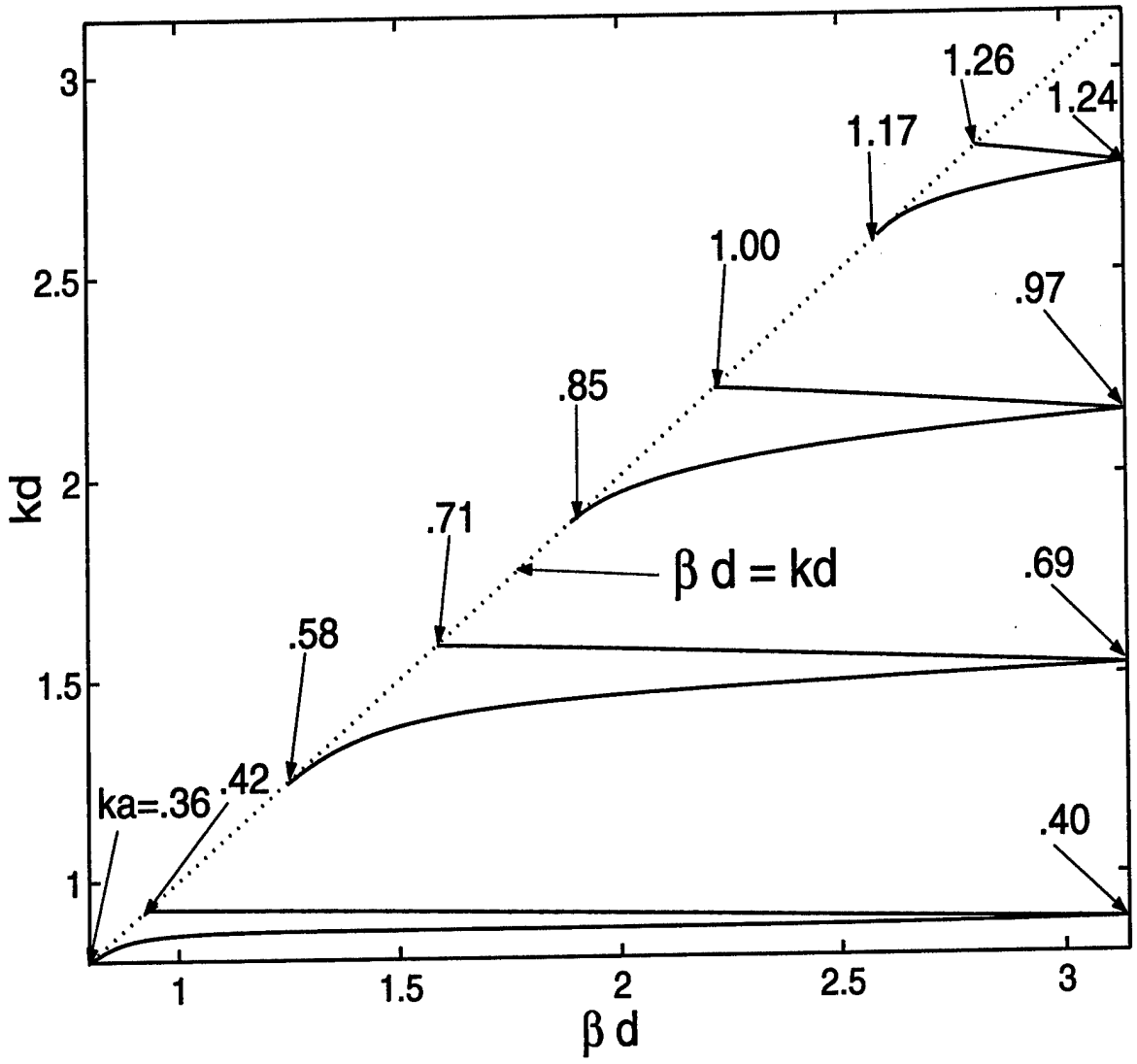

Figure 12: kd — βd diagram for a traveling wave on an infinite linear periodic array of spheres with $\epsilon_r = 10, \mu_r = 10$, and $a/d = 0.45$.

for a linear array of lossless homogeneous spheres with $\epsilon_r = 10, \mu_r = 10$, and $a/d = 0.45$. (The dotted line shows $\beta d = kd$.) We note that there are four sections of the $kd - \beta d$ diagram, each section corresponding to a narrow window of ka in the vicinity of one of the resonances of the Mie scattering coefficients of a_1^{sc} and b_1^{sc} at $ka = 0.405, 0.693, 0.988$, and 1.299; see Figure 3. Each section begins and ends when $\beta d \approx kd$. It is of considerable interest that each of the four sections consists of two branches, the lower branch with βd increasing from kd to π as kd increases, and the upper branch with βd decreasing from π to kd as kd continues to increase. The phase velocity of the traveling wave is positive on both branches while the group velocity ($\mathrm{d}k/\mathrm{d}\beta$) of the traveling wave is positive on the lower branch and negative on the upper branch. Hence the traveling waves corresponding to the upper branches of the four sections of $kd - \beta d$ diagram are "backward" traveling waves.

Our understanding of the $kd - \beta d$ diagram of Figure 12 can be increased by extending the diagram to include values of βd between π and 2π. In Figure 13 we show the lowest of the four sections of the $kd - \beta d$ of Figure 12 extended to $\beta d > \pi$. (The dotted line is, as in Figure 12, the plot of $\beta d = kd$.) As we have commented at the end of Section 5, if $\pi < \beta d < 2\pi$ then β is the propagation constant of a fast traveling wave in the positive z direction, $\exp(\mathrm{i}\beta z)$, and β' with $0 < \beta' d = 2\pi - \beta d < \pi$ is the propagation constant of the corresponding slow traveling wave in the negative z direction, $\exp(-\mathrm{i}\beta' z)$. The dashed portions of the plots corresponding to $\beta d > \pi$ are thus simply mirror images in the line $\beta d = \pi$ of the solid portions of the plots for $0 < \beta d < \pi$. In general there is thus no need to show the $kd - \beta d$ diagram for values of $\beta d > \pi$ Here, however, what we can see from Figure 13 is that by extending the $kd - \beta d$ diagram to include values of $\beta d > \pi$ we obtain two curves, one consisting of the lower solid segment and the upper dashed segment, and the other consisting of the upper solid segment and the lower dashed segment. Either curve can be used to obtain the other by making use of the mirror symmetry. The slopes of these two curves are continuous at $\beta d = \pi$. The upper solid segment corresponds to a backward traveling wave since the group velocity, proportional to the slope of the curve, has the opposite sign of the direction of propagation of the slow wave. The group velocity of the slow traveling wave in the positive z direction whose $kd - \beta d$ diagram is the lower solid segment is very small in the interval between $ka = 0.3925$ and 0.3928.

As another example of the $kd - \beta d$ diagram obtained when the ratio of the sphere radius to the inter-sphere separation distance is held constant and the frequency varied, Figure 14 shows the $kd - \beta d$ diagram corresponding to Figure 12 when $\epsilon_r = 20 = \mu_r = 20$ instead of 10; $a/d = 0.45$ as before. There are now nine sections of the $kd - \beta d$ diagram instead of four, corresponding to the more densely spaced resonances of the Mie scattering coefficients of a_1^{sc} and b_1^{sc} at $ka = 0.214, 0.366, 0.516, 0.665, 0.816, 0.968, 1.122, 1.279$, and 1.437. Although otherwise the $kd - \beta d$ diagrams appear to be similar, there is an interesting new feature of the two lower branches of the $kd - \beta d$ diagram of Figure 14 not present in any of the branches of the $kd - \beta d$ diagram of Figure 12 or the higher branches of Figure 14. This feature can be seen clearly in Figure 15 which shows in detail the behavior of the lowest branch of Figure 14. We note that as the branch is traced out from its beginning at $ka = 0.2098$ and $kd = 0.4662$ to its end at $ka = 0.2166$ and $kd = 0.4813$ that ka and kd are not monotonic increasing as they are for all the branches of the $kd - \beta d$ diagram of Figure 12 and all but the two lowest branches of Figure 14. Instead, ka first increases from 0.2098 to 0.2140, then decreases to 0.2107, and then increases monotonically to 0.2166. As a consequence of this behavior, in

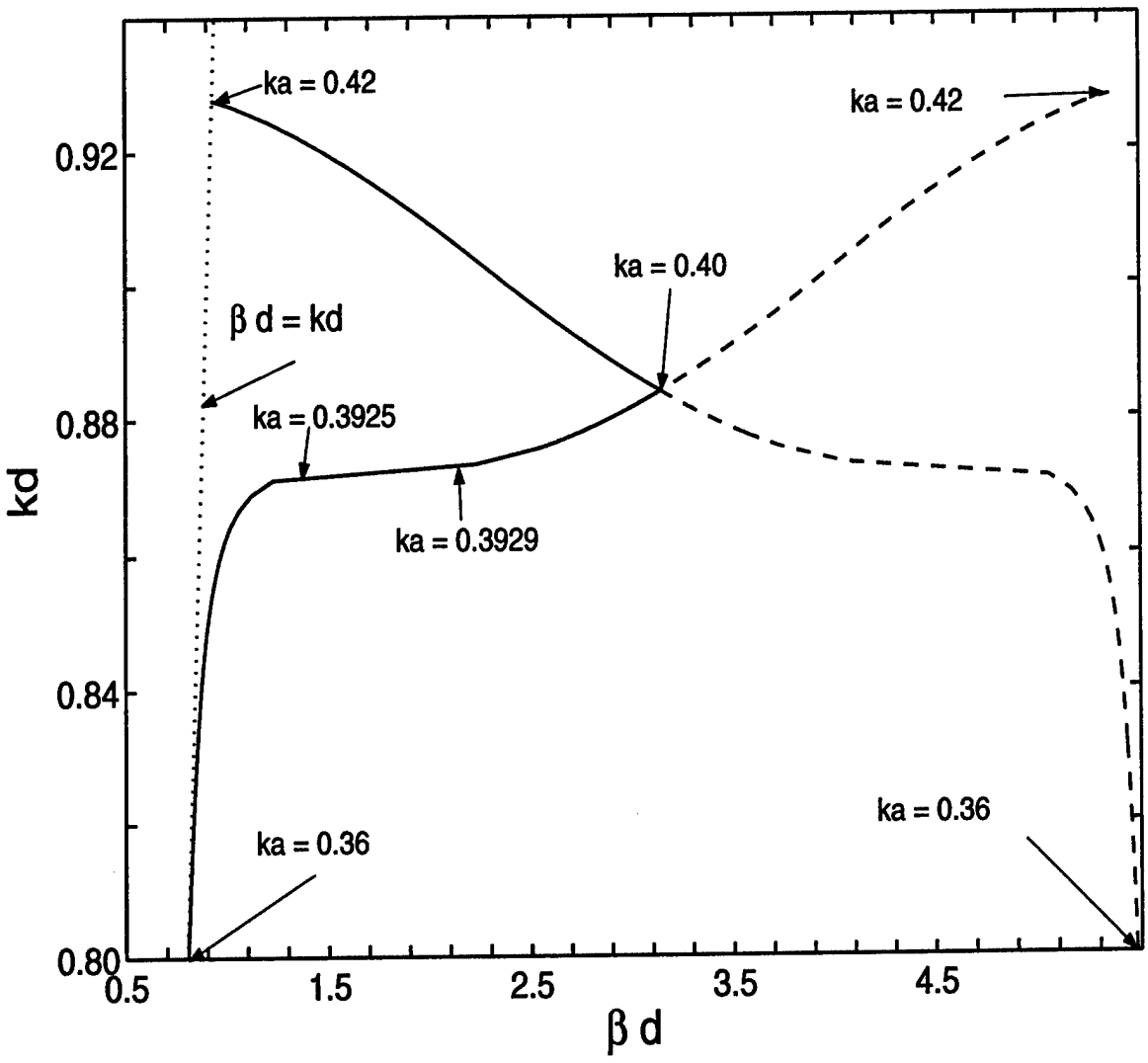

Figure 13: kd — βd diagram for a traveling wave on an infinite linear periodic array of spheres with $\epsilon_r = 10, \mu_r = 10$, and $a/d = 0.45$.

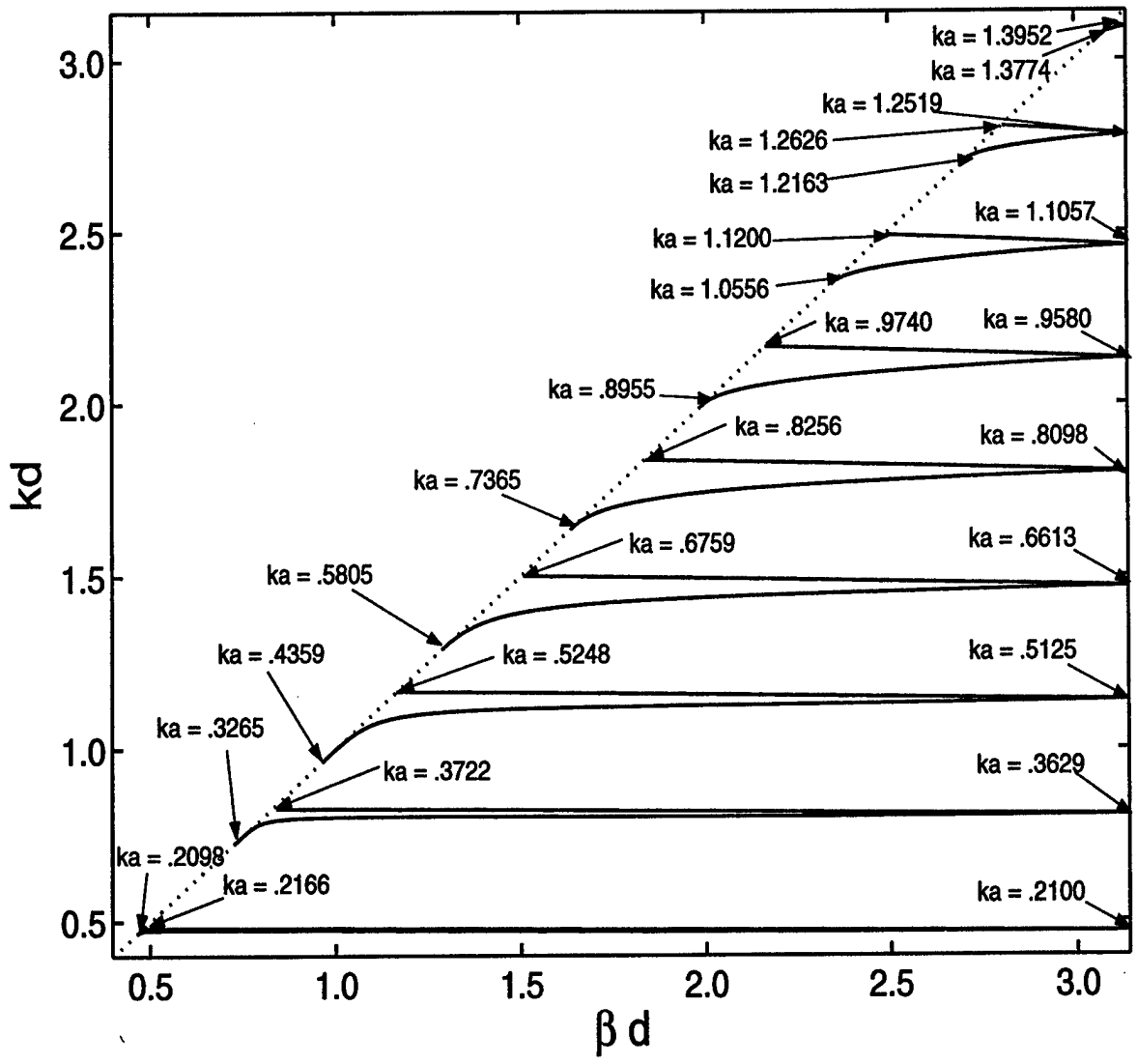

Figure 14: kd — βd diagram for a traveling wave on an infinite linear periodic array of spheres with $\epsilon_r = 20, \mu_r = 20$, and $a/d = 0.45$.

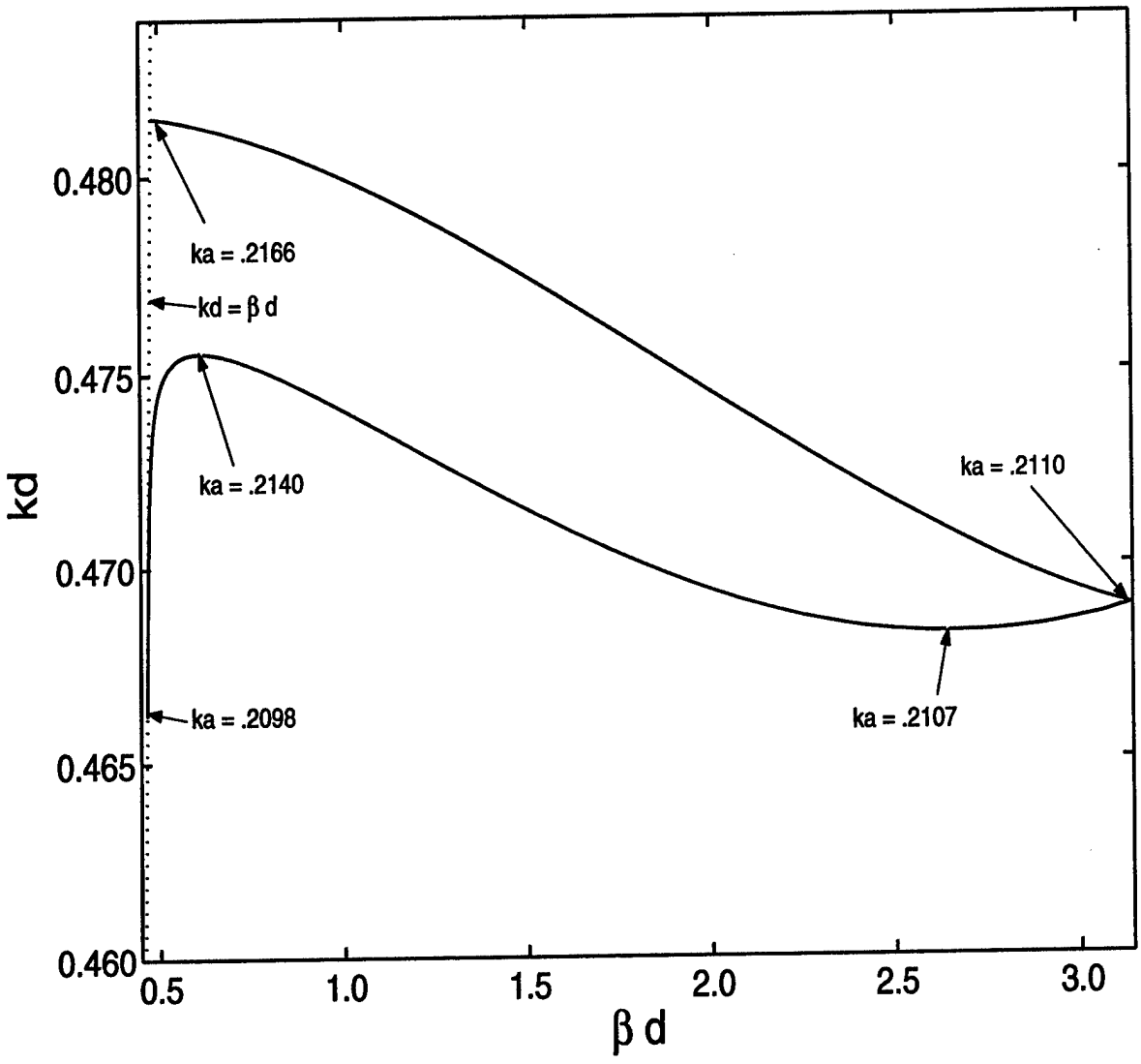

Figure 15: Lowest branch of the kd — βd diagram for a traveling wave on an infinite linear periodic array of spheres with $\epsilon_r = 20, \mu_r = 20$, and $a/d = 0.45$.

the interval of the electric spacing of the spheres, kd, from 0.4682 to 0.4756, there is not just one corresponding value of the traveling wave propagation constant βd but three. In other words, the array can support three distinct traveling waves for kd in this interval. Also, note that this branch of the $kd-\beta d$ diagram displays negative group velocity for ka between 0.2140 and 0.2107, and for ka between 0.2110 and 0.2166, and positive group velocity elsewhere. Similar behavior, though less pronounced, is exhibited by the next-to-lowest branch of the $kd-\beta d$ diagram of Figure 14, as shown in Figure 16.

The $kd-\beta d$ curves shown in Figures 12-16 have been for arrays of lossless magnetodielectric spheres. It is also of interest to show some examples of $kd-\beta d$ curves for linear arrays of lossless dielectric spheres ($\mu_r = 1$). In Figure 17 we show the $kd-\beta d$ curve for an array of dielectric spheres with $\epsilon_r = 10$ and $a/d = 0.4$. For small kd and ka there is very little scattering between the spheres and the $kd-\beta d$ curve very closely follows the $kd = \beta d$ line, meaning that the traveling wave is very loosely bound to the array. When ka starts to approach the first resonance of the first magnetic Mie coefficient at $ka = 0.951$ (see Figure 5), scattering between the spheres increases and a slow traveling wave can be supported by the array. The upper branch of the $kd-\beta d$ curve corresponds to values of ka for which both the first magnetic and first electric Mie coefficients are about 4 dB below their first resonance peaks. In Figure 18 the $kd-\beta d$ curve is shown for a linear array of the same dielectric spheres, $\epsilon_r = 10$, but with $a/d = 0.3$. The lower branch of the $kd-\beta d$ curve is similar in shape to that of the lower branch of the $kd-\beta d$ curve in Figure 17. The very small upper branch has a negative slope and corresponds to a backward traveling wave.

8 CONCLUDING REMARKS

In this report we have used the source scattering-matrix framework to investigate dipolar traveling waves that can be supported on infinite linear periodic arrays of lossless penetrable (magnetodielectric) spheres. The report focuses on obtaining the $kd-\beta d$ diagrams for these traveling waves.

In future work we will attempt to extend the analysis of linear periodic arrays of penetrable spheres given in this report to two- and three-dimensional periodic arrays of lossless penetrable spheres. Such an extention is highly worthwhile in view of the facts that a doubly negative (DNG) medium can be formed by embedding a 3D array of spherical particles in a background medium and that backward waves have been shown in this report to be supported by linear arrays of spheres with appropriately chosen permittivity and permeability. The starting point for this extension is equations (32a, 32b), and equations (33a, 33b) which give the scattered electric and magnetic dipole fields resulting from an $\hat{\mathbf{x}}$ directed electric field and a $\hat{\mathbf{y}}$ magnetic field incident on a penetrable sphere. These equations then lead to equations analogous to (37) and (39). Instead of the linear sums in (37) and (39), however, the analogous 2D and 3D array equations will contain double and triple summations representing the contributions of the scattered electric and magnetic fields of the spheres in the 2D and 3D arrays to the electric and magnetic fields incident on a given sphere in the array. It remains to be seen whether the complications resulting from these double and triple summations can be successfully treated.

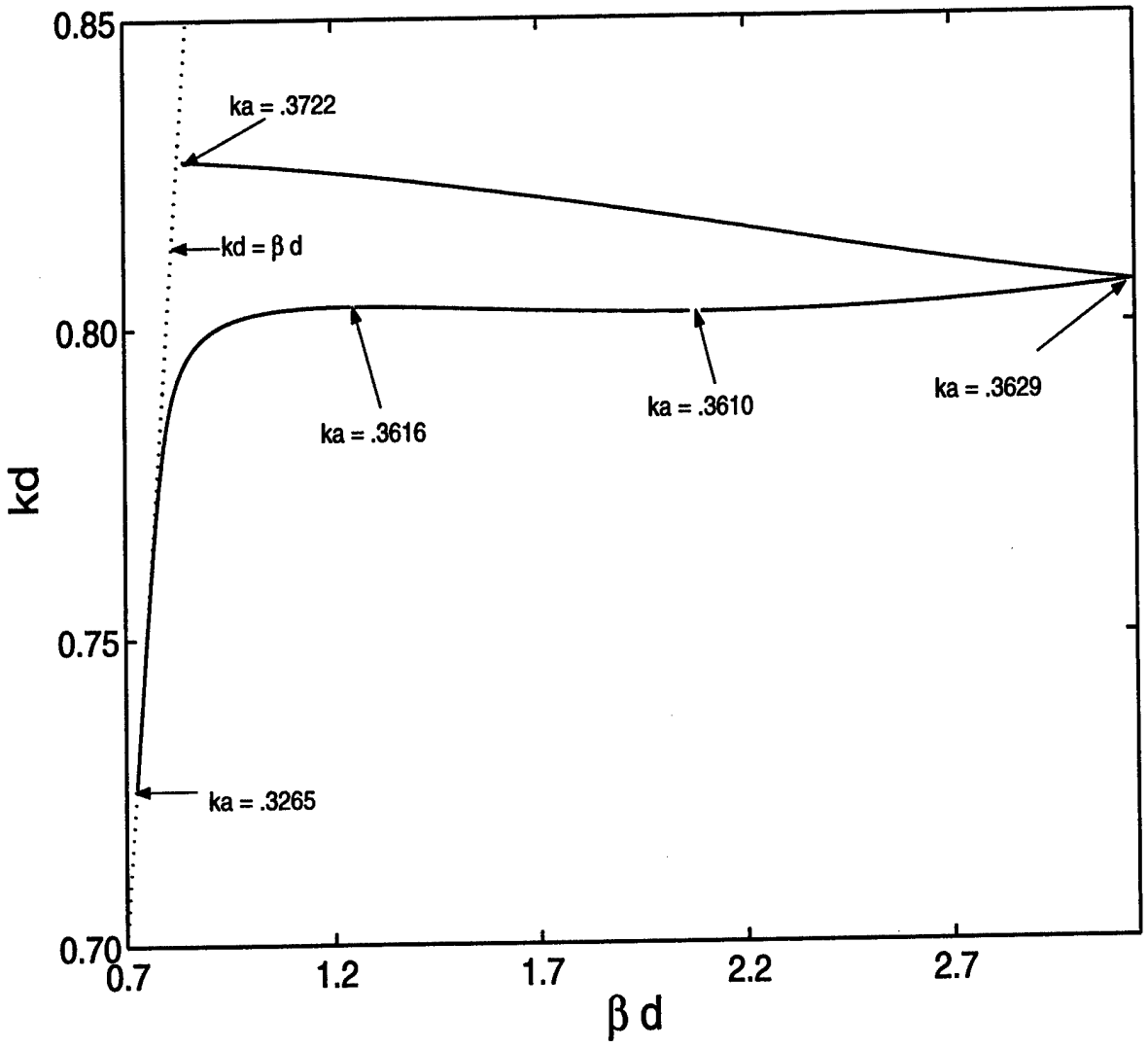

Figure 16: Next-to-lowest branch of the kd — βd diagram for a traveling wave on an infinite linear periodic array of spheres with $\epsilon_r = 20, \mu_r = 20$, and $a/d = 0.45$.

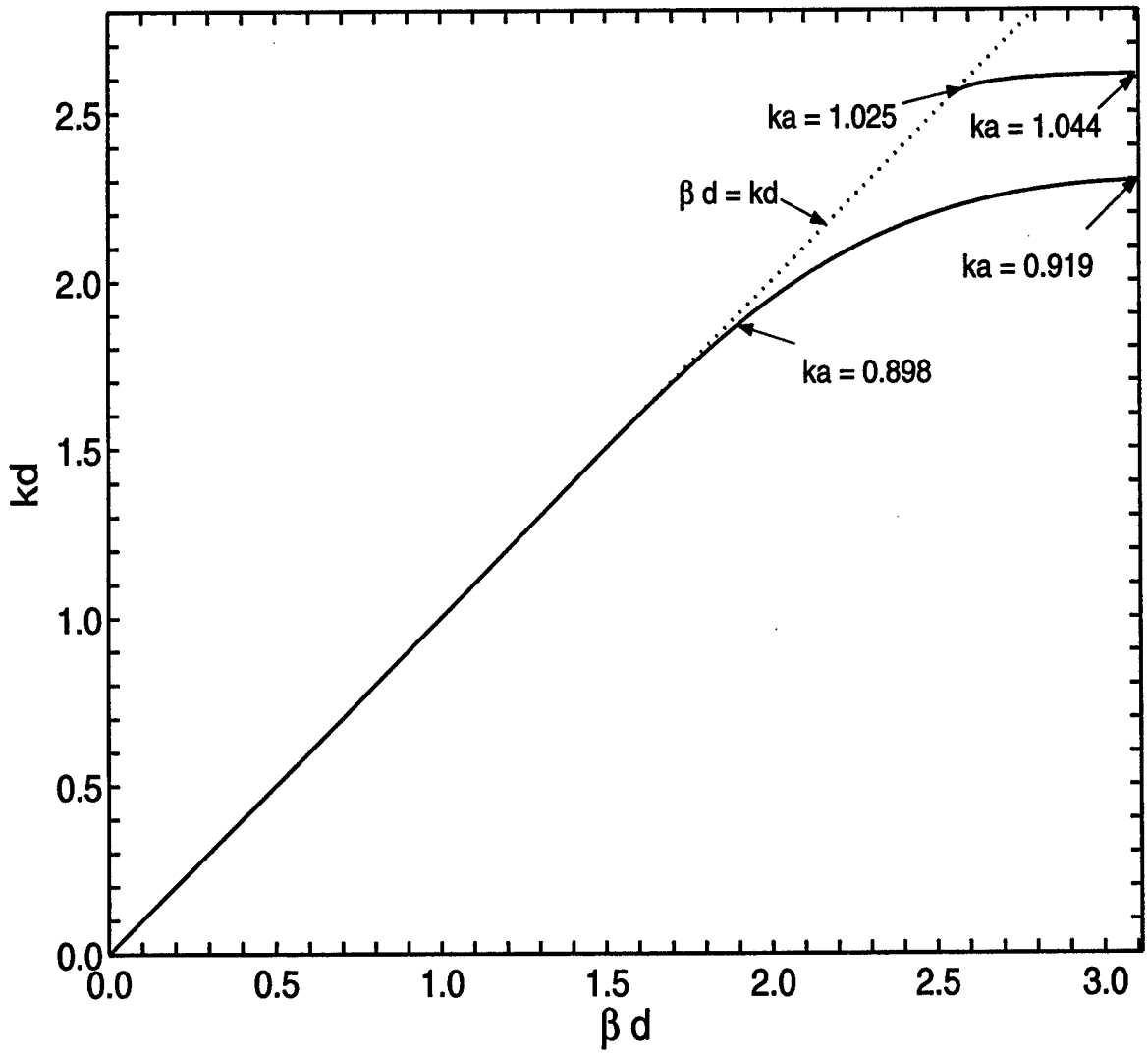

Figure 17: kd — βd diagram for a traveling wave on an infinite linear periodic array of spheres with $\epsilon_r = 10, \mu_r = 1$, and $a/d = 0.4$.

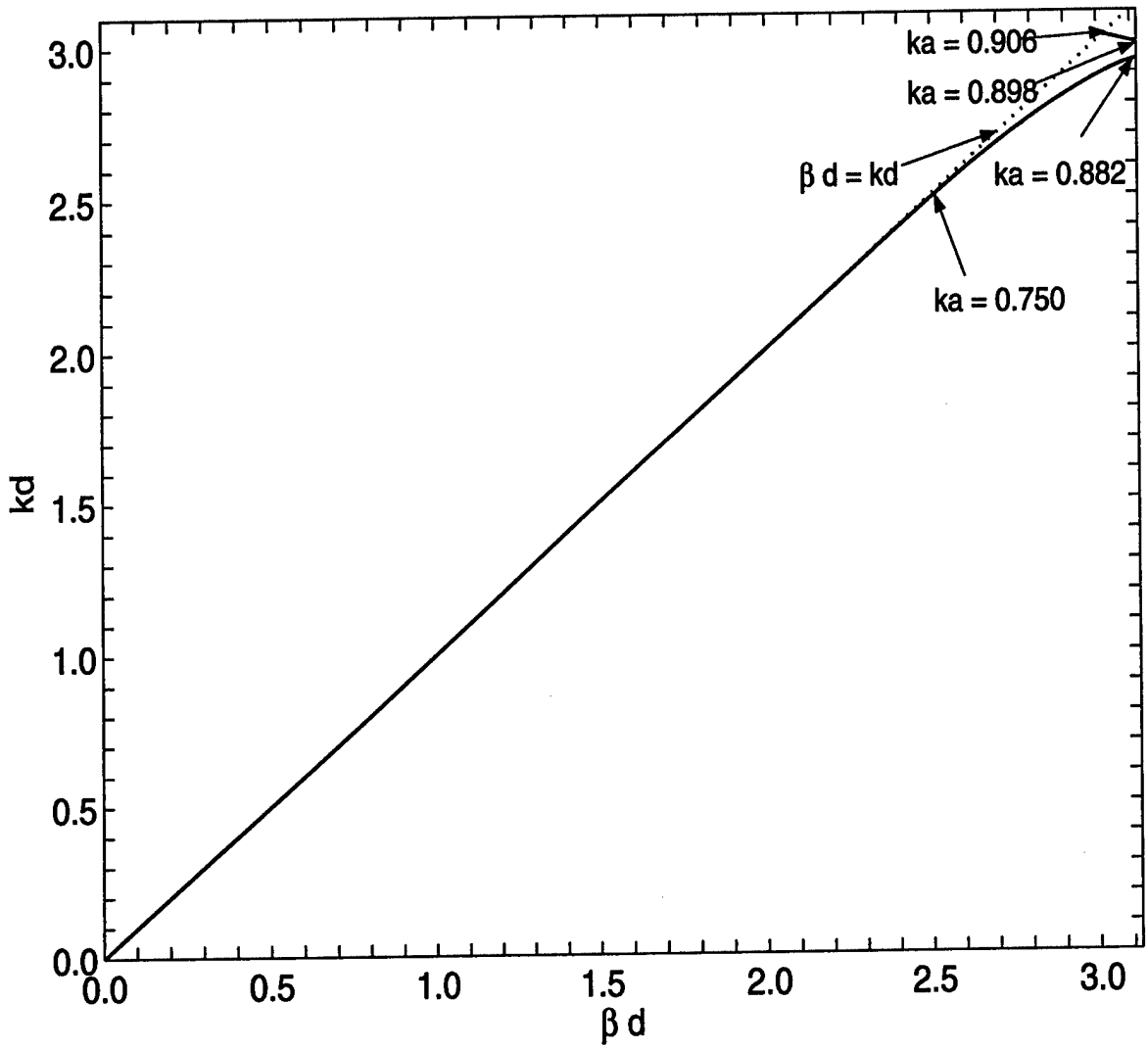

Figure 18: kd — βd diagram for a traveling wave on an infinite linear periodic array of spheres with $\epsilon_r = 10, \mu_r = 1$, and $a/d = 0.3$.

A VECTOR SPHERICAL WAVE FUNCTIONS

In this Appendix we give the definitions of the vector spherical wave functions **M** and **N** used in this report. The definitions are those used by Billy Brock [7] adapted for the $\exp(-i\omega t)$ time dependence used here:

$$\mathbf{M}_{lm}^{(i)}(\mathbf{r}) = i\sqrt{\frac{(2l+1)(l-m)!}{4\pi l(l+1)(l+m)!}} \left[\begin{array}{l} \dfrac{im}{\sin\theta} z_l^{(i)}(kr) P_l^m(\cos\theta) e^{i\phi}\hat{\boldsymbol{\theta}} \\ \\ +\sin\theta z_n^{(i)}(kr) \dfrac{d}{dx} P_l^m(x)\Big|_{x=\cos\theta} e^{im\phi}\hat{\boldsymbol{\phi}} \end{array} \right], \tag{64}$$

$$\mathbf{N}_{lm}^{(i)}(\mathbf{r}) = i\sqrt{\frac{(2l+1)(l-m)!}{4\pi l(l+1)(l+m)!}} \left\{ \begin{array}{l} \dfrac{z_l^{(i)}(kr)}{kr} l(l+1) P_l^m(\cos\theta) e^{im\phi}\hat{\mathbf{r}} \\ \\ -\dfrac{1}{kr}\dfrac{\partial}{\partial r}\left[r z_l^{(i)}(kr)\right] \sin\theta \dfrac{d}{dx} P_l^m(x)\Big|_{x=\cos\theta} e^{im\phi}\hat{\boldsymbol{\theta}} \\ \\ +\dfrac{1}{kr}\dfrac{\partial}{\partial r}\left[r z_l^{(i)}(kr)\right] \dfrac{im}{\sin\theta} P_l^m(\cos\theta) e^{im\phi}\hat{\boldsymbol{\phi}} \end{array} \right\}. \tag{65}$$

In (64) and (65) $z_l^{(1)}$ and $z_l^{(2)}$ are the spherical Bessel and Hankel functions j_l and $h_l^{(1)}$, respectively, and $P_l^m(x)$ is the associated Legendre function given by

$$P_l^m(x) = (-1)^m (1-x^2)^{m/2} \frac{d^m}{dx^m} P_l(x), m > 0, \tag{66a}$$

$$P_l^{-|m|}(x) = (-1)^m \frac{(n-m)!}{(n+m)!} P_l^m(x), m > 0, \tag{66b}$$

where $P_l(x)$ is the Legendre function

$$P_l(x) = \frac{1}{2^l l!} \frac{d^l}{dx^l}(x^2-1)^l. \tag{67}$$

The vector spherical wave functions **M** and **N** given by (64) and (65) can be defined in terms of the normalized radially-independent vector spherical harmonic function $\mathbf{X}_{lm}$ of Jackson [6] by

$$\mathbf{M}_{lm}^{(i)}(\mathbf{r}) \equiv z_l^{(i)}(kr)\mathbf{X}_{lm}(\theta,\phi) \tag{68}$$

and

$$\mathbf{N}_{lm}^{(i)}(\mathbf{r}) \equiv \frac{1}{k}\nabla \times z_l^{(i)}(kr)\mathbf{X}_{lm}(\theta,\phi), \tag{69}$$

and are related to the $\mathbf{F}_{1lm}^{(c)}$ and $\mathbf{F}_{2lm}^{(c)}$ vector spherical wave functions of Hansen [15] by

$$\mathbf{M}_{lm}^{(i)}(\mathbf{r}) = i\mathbf{F}_{1ml}^{(c)}(\mathbf{r}) \tag{70}$$

and

$$\mathbf{N}_{lm}^{(i)}(\mathbf{r}) = i\mathbf{F}_{2ml}^{(c)}(\mathbf{r}) \tag{71}$$

where the superscript $i = 1$ when $c = 1$ and the superscript $i = 2$ when $c = 3$.[2]

[2]These relations between the vector spherical harmonics of Brock and those of Hansen are given incorrectly in the original form of [7] but have been corrected by Brock in an errata.

B SUMMATIONS OF TRIGONOMETRIC SERIES

In this Appendix we discuss the approximations used for the sums of the trigonometric series

$$F(a) \equiv \sum_{j=1}^{\infty} \frac{\sin ja}{j^2}, 0 < a < \pi \tag{72a}$$

and

$$G(a) \equiv \sum_{j=1}^{\infty} \frac{\cos ja}{j^3}, 0 < a < \pi. \tag{72b}$$

Closed form expressions are not available for these sums. The IMSL least-squares approximation program FNLSQ was used to compute the approximations

$$F(a) \approx -0.1381 \sin a + 0.03212 \sin 2a - 0.9653a \ln(a/\pi), \quad 0 < a < \pi \tag{73a}$$

and

$$G(a) \approx 1.3328 - 0.1424 \cos a + 0.01094 \cos 2a + 0.4902a^2 \ln(a/\pi) - 0.2417a^2, \quad 0 < a < \pi. \tag{73b}$$

Figures 19 and 20 show F(a) and G(a), respectively, calculated with 1000 terms, along with their least squares approximations. The agreement of the approximate with the exact curves is excellent. It will be noted that although $G'(a) = -F(a)$, when the approximation for $G(a)$ is differentiated the result differs slightly from the negative of the derivative of the approximation for $F(a)$. While it is possible to obtain an approximation for $F(a)$ by taking the negative of the derivative of the approximation for $G(a)$, the direct least-squares fit approximation for $F(a)$ that we have used distributes the errors in the approximation more uniformly over the interval from 0 to π.

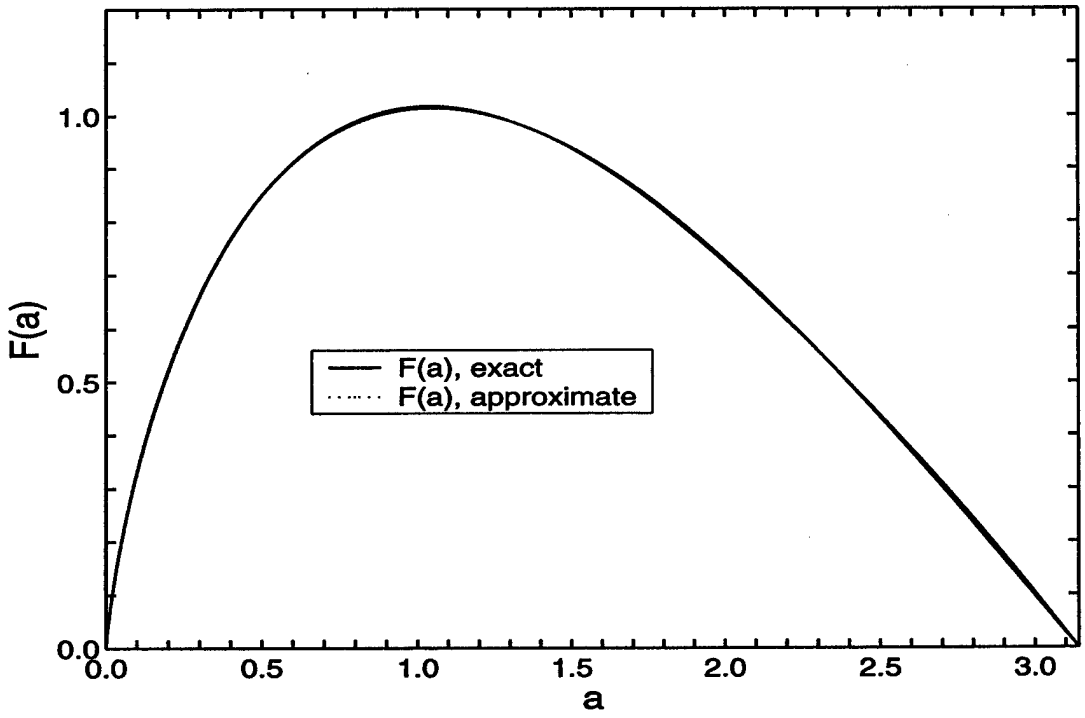

Figure 19: $F(a) \equiv \sum_{j=1}^{\infty} \frac{\sin na}{n^2}$, $0 < a < \pi$, exact and approximate.

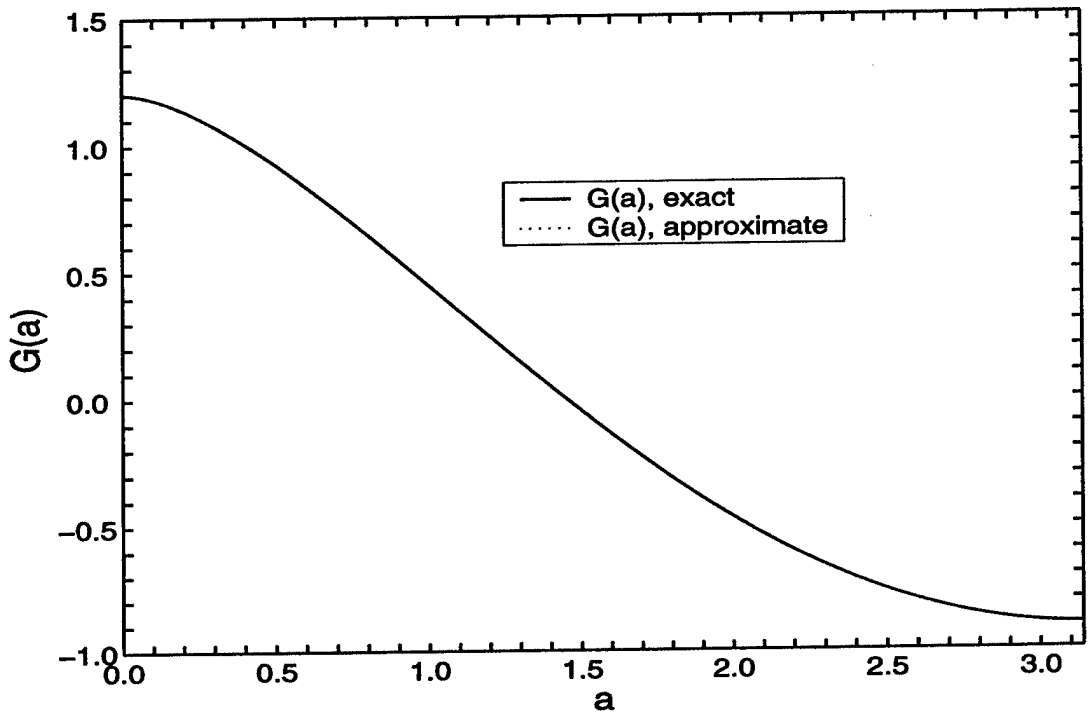

Figure 20: $G(a) \equiv \sum_{j=1}^{\infty} \frac{\cos na}{n^3}$, $0 < a < \pi$, exact and approximate.

References

[1] A.D. Yaghjian, "Scattering-Matrix Analysis of Linear Periodic Arrays," *IEEE Trans. Antennas Propagat.*, vol. 50, pp. 1050–1064, August 2002.

[2] R.A. Shore and A.D. Yaghjian, *Scattering-Matrix Analysis of Linear Periodic Arrays of Short Electric Dipoles*, Air Force Research Laboratory In-House Report, AFRL-SN-HS-TR-2004-045, 2004.

[3] L. Lewin, "The electrical constants of a material loaded with spherical particles," *Proc. IEE*, vol. 94, pp. 65–68, 1947.

[4] P.C. Waterman and N.E. Pedersen, "Electromagnetic scattering by periodic arrays of particles," *J. Appl. Phys.*, vol. 59, pp. 2609–2618, 1986.

[5] C.L. Holloway et al., "A double negative (DNG) composite medium composed of magnetodielectric spherical particles embedded in a matrix," *IEEE Trans. Antennas Propagat.*, vol. 51, pp. 2596–2603, October 2003.

[6] J.D. Jackson, *Classical Electrodynamics, 3rd Edition*, New York: Wiley, 1999.

[7] B.C. Brock, *Using Vector Spherical Harmonics to Compute Antenna Mutual Impedance from Measured or Computed Fields*, Sandia Report SAND2000-2217, Sandia National Laboratories, September, 2000. Available on the web at http://www.prod.sandia.gov/cgi-bin/techlib/access-control.pl/2000/002217r.pdf

[8] A.D. Yaghjian, *Near-Field Measurements on a Cylindrical Surface: A Source Scattering-Matrix Formulation*, NBS Technical Note 696, Boulder, CO, September 1977.

[9] J. Appel-Hansen, E.S. Gillespie, T.G. Hickman, and J.D. Dyson, "Antenna Measurements," ch. 8 in *The Antenna Design Handbook, Vol. 1*, Eds. A.W. Rudge, K. Milne, A.D. Olver, and P. Knight, London: Peregrinus, 1982.

[10] C.G. Montgomery and R.H. Dicke, "Waveguide Junctions with Several Arms," ch. 9 in *Principles of Microwave Circuits*, Eds. C.G. Montgomery, R.H. Dicke, and E.M. Purcell, New York: McGraw-Hill, 1948.

[11] J.A. Stratton, *Electromagnetic Theory*, New York: McGraw-Hill, 1941.

[12] H.C. Van De Hulst, *Light Scattering by Small Particles*, New York: John Wiley, 1957.

[13] I.S. Gradshteyn and I.M. Ryzhik, *Table of Integrals, Series, and Products; 5th Edition*, Boston: Academic, 1994.

[14] C.F. Bohren and D.R. Huffman, *Absorption and Scattering of Light by Small Particles*, New York: John Wiley, 1983.

[15] J.E. Hansen, Ed., *Spherical Near-Field Antenna Measurements*, London: Peregrinus, 1988.